Order Number 1353683

Neutron irradiation effects on the breakdown voltage of power MOSFETs

Hasan, Samil Mukhlisin Yauma, M.S.

The University of Arizona, 1993

U·M·I
300 N. Zeeb Rd.
Ann Arbor, MI 48106

NEUTRON IRRADIATION EFFECTS ON THE BREAKDOWN VOLTAGE OF POWER MOSFETS

by
Samil Mukhlisin Yauma Hasan

A Thesis Submitted to the Faculty of the

DEPARTMENT OF ELECTRICAL AND COMPUTER ENGINEERING

In Partial Fulfillment of the Requirements
For the Degree of

MASTER OF SCIENCE
WITH A MAJOR IN ELECTRICAL ENGINEERING

In the Graduate College

THE UNIVERSITY OF ARIZONA

1993

STATEMENT BY AUTHOR

This thesis has been submitted in partial fulfillment of requirements for an advanced degree at The University of Arizona and is deposited in the University Library to be made available to borrowers under rules of the Library.

Brief quotations from this thesis are allowable without special permission, provided that accurate acknowledgement of source is made. Requests for permission for extended quotation from or reproduction of this manuscript in whole or in part may be granted by the copyright holder.

SIGNED: 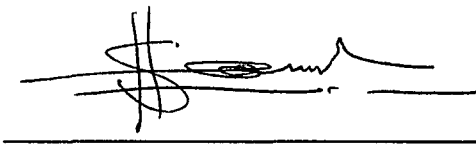

APPROVAL BY THESIS DIRECTOR

This thesis has been approved on the date shown below:

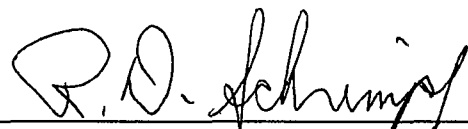

Ronald D. Schrimpf
Associate Professor of
Electrical and Computer Engineering

7/30/93
Date

ACKNOWLEDGEMENTS

My deepest thanks go to my advisor, Dr. Ronald Schrimpf, whose patience, trust, support, and guidance since my undergraduate years have been invaluable and encouraging.

I would like to thank Dr. Kenneth Galloway whose support and guidance throughout my masters program have pushed me to give my best.

I would like to thank Dr. John Williams and his staff from the Nuclear Engineering Department, the University of Arizona, for their assistance in using the radiation facility. Special thanks go to Mr. Harry Doane for his assistance during neutron irradiation experiments.

Also, I would like to thank Jeff Titus of the Naval Surface Warfare Center for information about some device dimensions used in the experiment.

I would like to thank all my friends in the Radiation Effects Group for their valuable help and discussion.

Lastly, but not the least, I would like to thank both my parents whose long distance guidance makes me strong during difficult times.

TABLE OF CONTENTS

LIST OF FIGURES

LIST OF FIGURES CONTINUED

LIST OF TABLES

ABSTRACT

The effect of neutron radiation on power MOSFET breakdown voltage has been investigated. Power metal-oxide-semiconductor field effect transistors (power MOSFETs) of both n- and p-channel with manufacturer's rated breakdown voltage between 100 to 500V were radiated using the TRIGA Neutron Irradiation Facility of the Nuclear Engineering Department, the University of Arizona. Accumulated neutron fluence effects up to $5x10^{14}$ neutron/cm^2 were investigated. Considerable increase in the breakdown voltages were observed in n-type MOSFETs after 10^{13} neutron/cm^2 and to p-type MOSFETs after 10^{12} neutron/cm^2. An increase in breakdown voltage of as much as 30% was observed after $5x10^{14}$ neutron/cm^2. The increase in breakdown voltages is due to the decrease in the mean free path caused by the neutron-irradiation-induced defects. The effect of positive trapped charge oxide due to concomitant gamma radiation and the effect of the termination structure to the breakdown voltage were considered. S-PISCES 2B device simulation was used to investigate the change in the b coefficient of Chynoweth's law that relates to the mean free path. Two empirical models are presented: one predicts the power MOSFET breakdown voltage after a certain amount of neutron fluence and the other considers the change in the b coefficient after some amount of neutron radiation to predict the change of breakdown voltage in a device simulation.

CHAPTER 1

INTRODUCTION

1.1 Motivation

Power metal-oxide-semiconductor field effect transistors or power MOSFETs have important applications in environments that may expose them to high neutron fluences. The applications include nuclear power plants and military systems. This work examines the effects of neutron irradiation on the breakdown voltage of power MOSFETs.

Power MOSFETs have many advantages over their power bipolar junction transistor (power BJT) counterparts. MOSFETs are majority carrier devices. They are not affected by minority-carrier charge storage; hence, they make faster switching circuits. At a frequency of 100 kHz, their power dissipation is about 5 times lower than power BJTs' [1]. This translates to lower cost, smaller size, and lighter weight of the reactive circuit components.

Power MOSFETs have simpler input drive requirements than power BJTs. The oxide insulator separating the gate from the body and the source makes the drive requirements nearly independent of the load current. The oxide gives very high DC resistance. The gate may be driven directly from a low power logic integrated circuit to control a high power circuit directly.

1.2 Power MOSFET Device Structure

Figure 1.1 shows the cross-sectional view of two adjacent cells of an n-channel power MOSFET [2]. Several hundreds or thousands of cells are connected in parallel to achieve high current rating. The epi-layer acts as the drain of the devices. The first p-type diffusion makes up the body region. A thin oxide layer, typically in the range of 40 to 100 nm, and a polysilicon gate above it complete the MOS structure. The source metalization usually shorts the source and the p-body regions. The channel is defined as the region under the silicon-silicon dioxide interface inside the p-body region. Although the power MOSFET structure is different from the conventional, lateral MOSFET structure (figure 1.2), the basic operating mechanisms are the same.

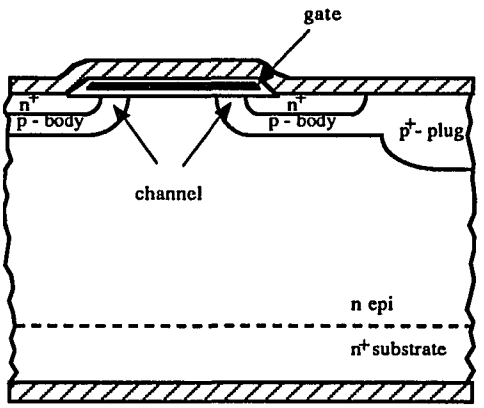

Figure 1.1 Power MOSFET device structure

A MOSFET is operated by controlling the channel region under the gate. For an n-channel enhancement mode device, when all the terminals are grounded, the channel

under the gate is normally not conducting. When a positive voltage is applied to the gate, some holes in the body under the interface are repelled.

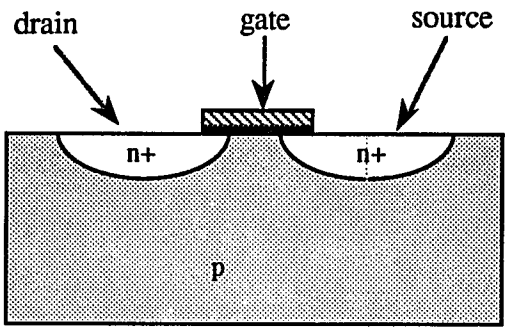

Figure 1.2 Lateral MOSFET Structure

If the gate voltage is increased high enough, some electrons begin to fill the channel. Inversion layer formation begins. If a voltage difference between the drain and the source exists, the drain current I_{DS} begin to flow and the channel conducts.

Conversely, if a negative bias is applied to the gate, more holes are attracted to the channel region and ideally only a small leakage current will flow between the drain and the source no matter how large V_{DS} is.

1.3 Breakdown Voltage

Three mechanisms are possible for p-n junction breakdown: thermal instability, tunneling, and avalanche multiplication [3, 4]. The thermal instability mechanism in a

semiconductor is important when the bandgap is small and saturation currents are high (e.g., Ge). The tunneling effect happens when breakdown voltages are less than about $4E_g/q$. For junctions with breakdown voltages more than $6E_g/q$, or approximately 6.7 V for Si, the avalanche multiplication mechanism is responsible [3]. Since all the transistors used in this work are MOSFETs with silicon substrates and manufacturer's breakdown ratings well beyond $6E_g/q$ (the smallest one is 100V), only the avalanche multiplication mechanism is considered here.

1.3.1 Avalanche Multiplication

When reverse bias voltage is applied across a p-n junction, it is supported across the depletion layer. Practically no voltage drops across the rest of the semiconductor exist. The electric field that exists across the depletion layer sweeps out any carriers that diffuse from the adjacent quasi-neutral regions or are created by space-charge region generation. The velocity of the mobile carriers is proportional to the electric field at relatively low values of electric field. Application of a higher voltage increases the electric field and accelerates the carriers to higher speed. The carrier velocity saturates at $1x10^7$ cm/s when the field is bigger than $1x10^5$ V/cm [1]. At higher electric fields, the mobile carriers colliding with lattice atoms can ionize the atoms creating electron-hole (e-h) pairs. Some of these electrons and holes have enough energy to create some more e-h pairs. The generation rate G for impact ionization is given by [4]

$$G = \alpha_n n v_n + \alpha_p p v_p \tag{1.1}$$

where $\alpha_{n(p)}$ is the electron (hole) ionization rate, *n(p)* is the electron *(hole)* density, and $v_{n(p)}$ is the electron (hole) velocity. The ionization rate is the number of e-h pairs generated per unit distance traveled by carriers inside the depletion region. The ratio of the carriers entering the depletion region to ones leaving the region is called the charge multiplication factor. When this factor becomes very large, avalanche breakdown happens.

1.3.2 Breakdown Voltage and Termination Structure

An ideal step junction, where one side is doped much higher than the other, empirically has breakdown voltage [4]

$$BV_{pp} = 5.34 \times 10^{13} N_{dop}^{-3/4} \tag{1.2}$$

where BV_{pp} is the ideal parallel plane breakdown voltage and N_{dop} is the doping density on the lowly doped side. The higher the voltage rating of the MOSFET, the lower the doping density of the epi-layer. Low doping density is usually undesirable due to its high resistivity, so the epi-layer is usually made as thin as possible to contain the depletion region of the reverse biased junction [5].

Electron and hole ionization rates inside the depletion region satisfy the empirical Chynoweth's law [6]

$$\alpha_{n(p)} = a_{n(p)} \exp\left(-\frac{b_{n(p)}}{E}\right) \tag{1.3}$$

where $a_{n(p)}$ is the ionization rate at infinite electric field E and $b_{n(p)}$ is the critical field constant for electrons (holes). Some work has been done on the coefficients of Chynoweth's law [7-9]. However, Temple and Adler [10] investigated avalanche breakdown in high voltage planar p-n junctions and found that only the coefficients of Van Overstraeten and De Man gave consistently accurate results for the structures they considered. The coefficients are [9]:

$a_n = 7.03 \times 10^5$ cm^{-1}

$b_n = 1.231 \times 10^6$ V/cm

for $1.75 \times 10^5 \leq E \leq 6.0 \times 10^5$ cm^{-1}

for electrons,

$a_p = 1.582 \times 10^6$ cm^{-1}

$b_p = 2.036 \times 10^6$ V/cm

for $1.75 \times 10^5 \leq E \leq 4.0 \times 10^5$ V/cm

and $a_p = 6.71 \times 10^5$ cm^{-1}

$b_p = 1.693 \times 10^6$ V/cm

for $4.0 \times 10^5 \leq E \leq 6.0 \times 10^5$ V/cm

for holes.

Shockley [11] predicted that $\alpha(E)$ was proportional to $exp(-E_i/qL_RE)$, where E_i was the ionization energy, q was the electronic charge, and L_R was the Raman phonon mean free path. Raman phonons refer to the highest frequency (energy) phonons for which the two face-centered-cubic (FCC) sub-lattices of the silicon diamond structure are vibrating in opposite directions. The model assumes only a few charges survive random collisions and gain enough energy to start impact ionization and that the dominant

scattering at high electric field in the structure is the phonon scattering. Comparing Shockley's prediction and Chynoweth's law, it is found that

$$b = \frac{E_i}{qL_R} \tag{1.4}$$

Thus, the critical electric field constant of Chynoweth's law depends on the value of the impact ionization energy and the collision mean free path.

Equation (1.2) has assumed an infinite parallel-plane p-n junction. In reality, the junction is terminated by regions of spherical or cylindrical curvature. Figure 1.3 shows the p^+-plug and n-epi regions where the breakdown of the device is most likely to happen. This device experiences electric field crowding at the regions of maximum junction curvature. This condition lowers the breakdown voltage significantly because higher electric field leads to larger impact ionization.

The effect of the cylindrical junction on breakdown voltage is given by [1]

$$\frac{BV_{cyl}}{BV_{pp}} = \left\{ \frac{1}{2}\left[\left(\frac{r_j}{W_c} \right)^2 + 2\left(\frac{r_j}{W_c} \right)^{6/7} \right] \ln\left[1 + 2\left(\frac{W_c}{r_j} \right)^{8/7} \right] - \left(\frac{r_j}{W_c} \right)^{6/7} \right\} \tag{1.5}$$

where BV_{cyl} = cylindrical junction breakdown voltage

BV_{pp} = parallel plane breakdown voltage

rj = junction curvature

W_C = depletion width at breakdown

With a typical value of $\frac{r_j}{W_c}$ between 0.1 and 0.2 , $\frac{BV_{cyl}}{BV_{pp}}$ is between 0.3 and 0.4. This is a very significant decrease.

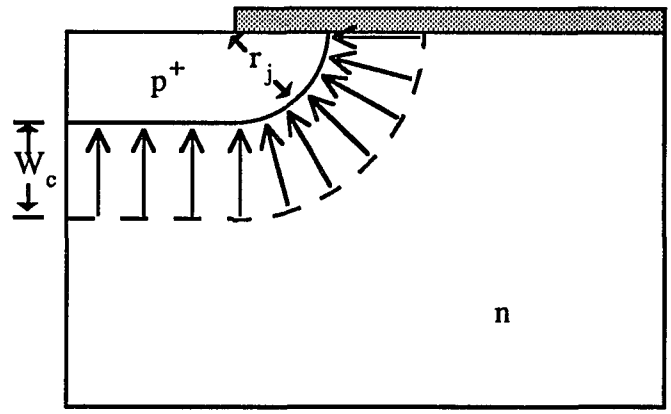

Figure 1.3 Electrical field crowding at cylindrical junction curvature

Most real devices have some termination structures that reduce the effect of the junction curvature. Two commonly used termination structures are floating field rings and field plates. Figure 1.4 shows the use of a one-field-ring termination structure. Figure 1.5 shows the use of a field plate termination. Several floating guard rings combined with a field plate or some other termination structures could be used together to approach the ideal parallel-plane breakdown voltage. Adler *et al* studied the breakdown voltage for planar devices with a single field limiting ring [12]. Then, Brieger, Gerlach, and Pelka [13] extended and offered an analytical model for devices with more than one field ring. Properly terminated devices can achieve more than 90% of the ideal breakdown voltage value [14,15].

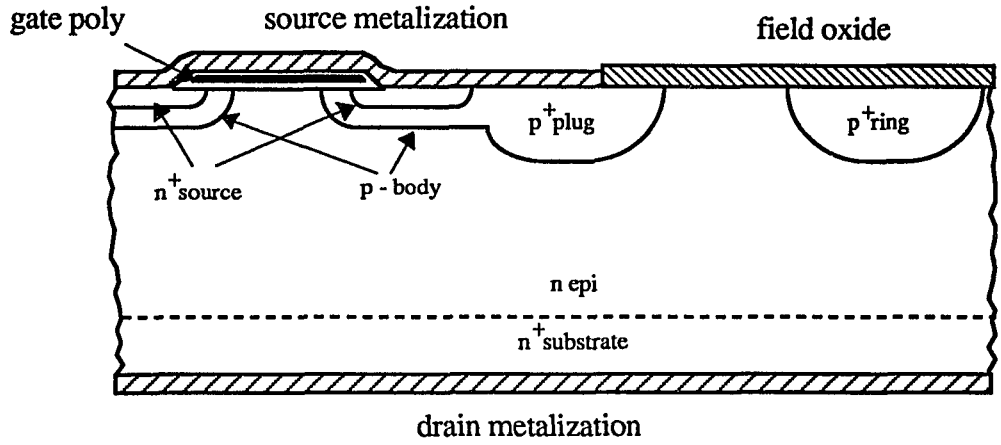

Figure 1.4 One field ring termination structure

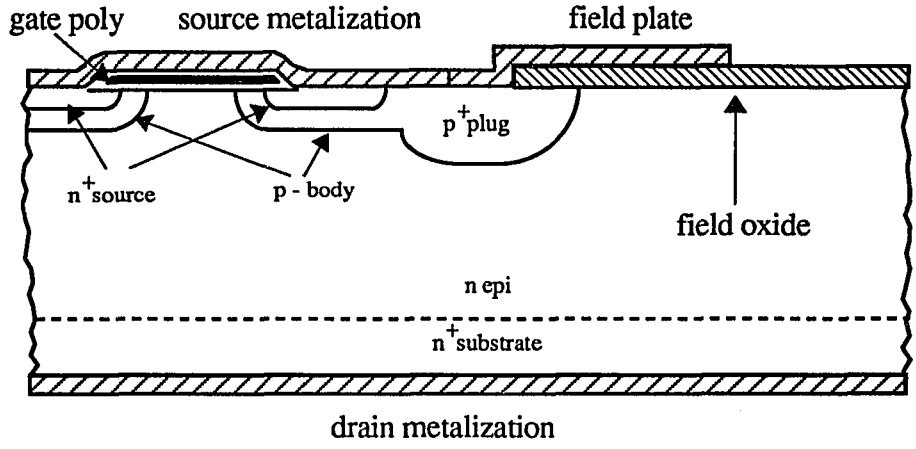

Figure 1.5 Field plate termination structure

Surface charge changes the depletion layer boundary, thus changing the electric field lines [16,17]. Figure 1.6 illustrates its effect on a p^+-n junction. In figure 1.6(a), negative charges deflect electrons near the interface, extending the depletion layer boundary. The electric field is less crowded so the breakdown voltage increases. Figure

1.6(b), illustrating positive surface charges, shows that electrons are attracted by the positive oxide charge, decreasing the breakdown voltage. Opposite effects happen in the case of an n^+-p junction: negative charges decrease the breakdown voltage and positive charges increase it.

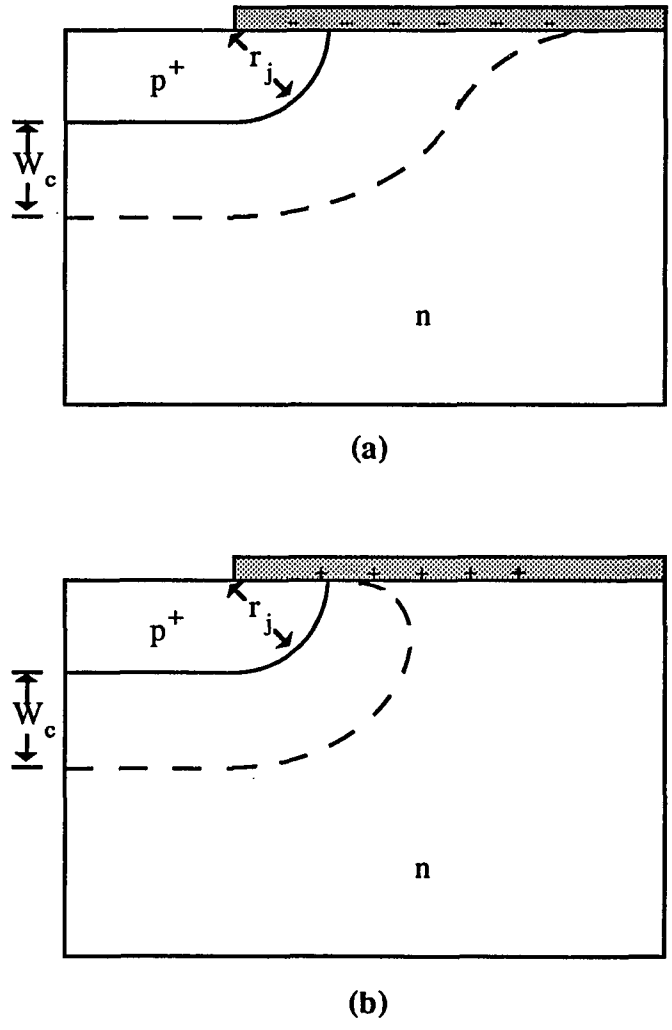

Figure 1.6 Effect of surface charges on the depletion region

In short, the breakdown voltage of a device depends on numbers of factors: doping density, junction depth, termination structure, surface charges, and the collision mean free path. These factors need to be considered in the investigation of the effect of neutron irradiation on the breakdown voltage of the power MOSFET.

CHAPTER 2

NEUTRON RADIATION INDUCED DAMAGE

A neutron is a fundamental sub-atomic particle with neutral charge. Neutron radiation affects a target through nuclear interactions only. Those interactions are: elastic scattering, inelastic scattering, and transmutation.

In an elastic collision, the incident neutron hits an atom of the target material, loses some energy to the atom and scatters. The process can dislodge the atom from its position (approximately 25 eV is needed for most materials [18, 19]). The displaced atom travels for a short distance, colliding and displacing other atoms, losing its energy to the displaced atoms or to ionization.

In inelastic scattering, the incident neutron is captured by the nucleus of the target atom momentarily and then released at lower energy. The nucleus is left excited and will return to its original state by emitting a gamma ray. An inelastic collision can also displace an atom from its lattice site.

In a transmutation reaction, the incident neutron is also captured by the nucleus of the target atom, but the captured neutron is not released. Rather, another particle such as a proton or an alpha particle is emitted leaving the remaining atom transmuted.

In many environments the neutrons involved have relatively high energy. The dominant processes involving high energy neutrons (fast neutrons) are elastic and inelastic scattering [18]. The mean free path of the neutron scattering is large compared to the thickness of wafers that devices are made, so the defects are uniform throughout the devices [20].

2.1 Displacement Damage Effects

2.1.1 Majority Carrier Removal

When an atom is displaced from its original lattice site, a frenkel defect is formed. A frenkel defect consists of a vacancy and an interstitial defect (see figure 2.1). Vacancies and interstitials can combine or interact with other vacancies or interstitials, or with impurity atoms to form defect complexes. All of these defects introduce energy levels in the energy band diagram.

Acceptor-like energy levels just above the valence band and below the fermi energy are effective in capturing electrons. Donor-like energy levels just below the conduction band and above the fermi energy are effective in capturing holes (see figure 2.2). These levels act as efficient majority carrier removal centers. After prolonged neutron irradiation, impurity doped silicon approaches intrinsic behavior due to the trapping of these levels (the conductivity approaches its intrinsic value: $4 \times 10^{-9}\ \Omega^{-1}\ cm^{-1}$) [21].

There are at least 29 different kinds of defects associated with the neutron irradiation. Each introduces a different energy level. Each also has a different creation rate

that depends on the temperature and fermi energy of the material [22]. Thus, it is difficult to analyze the effect of neutron irradiation based on the quantitative effect of each defect.

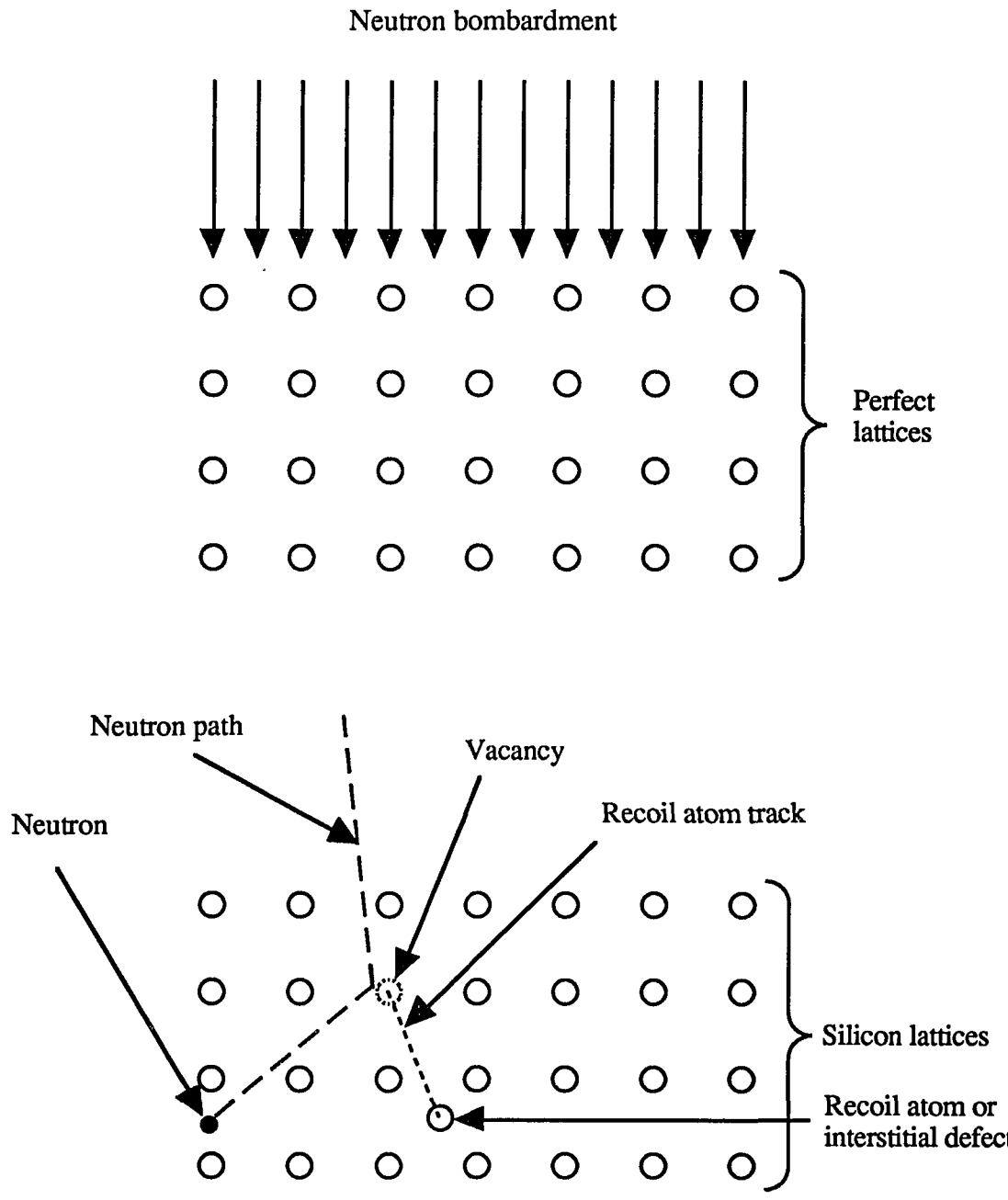

Figure 2.1 Neutron radiation and Frenkel defect formation

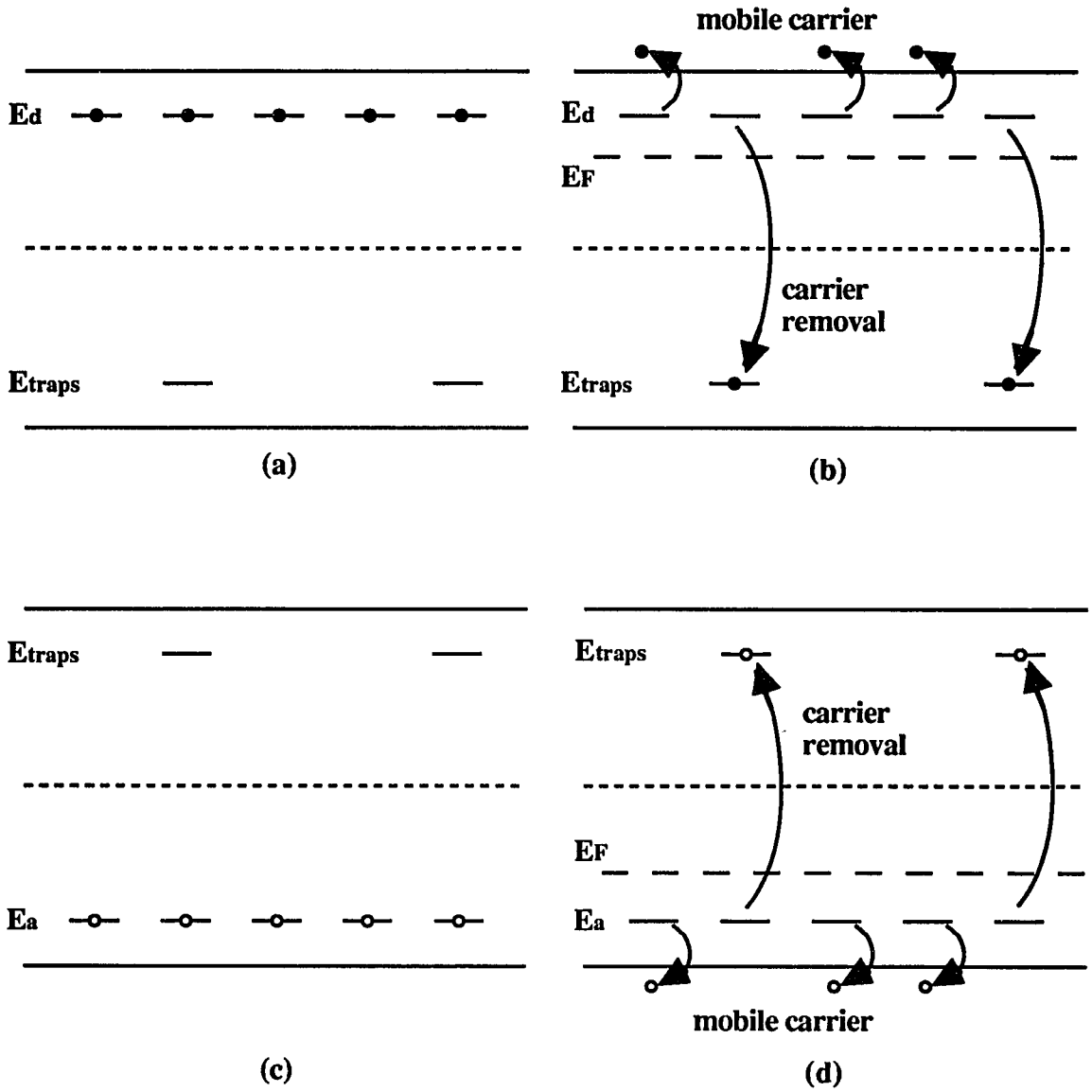

Figure 2.2 Majority carrier removal mechanisms: (a) freeze-out condition for n-type material, (b) room temperature condition for n-type material, (c) freeze-out condition for p-type material, (d) room temperature condition for p-type material.

Buehler [23] collected statistical data on the effect of neutron irradiation on the resistivity of p- and n-type silicon. He suggested empirical carrier removal equations due to the neutron irradiation. The resistivity ρ is related to the neutron fluence Φ by [23]

$$\rho_{n(p)} = \rho_{no(po)} \exp\left(\frac{\Phi}{k_{n(p)}}\right) \tag{2.1}$$

where $k_{n(p)}$ is the n-type (p-type) damage constant. These damage constants are functions of initial doping:

$$k_n = K_n n_o^{0.77} \tag{2.2-a}$$

$$k_p = K_p p_o^{0.77} \tag{2.2-b}$$

The coefficients K_n and K_p were given by Buehler [23] as 444 $cm^{0.31}$ and 387 $cm^{0.31}$, respectively.

Resistivity is related to carrier density by $\rho = (q\mu_n n + q\mu_p p)^{-1}$. For the relatively low doping density used in high power devices, the mobilities are relatively constant. Also, the change in mobility is negligible for neutron fluences up to 10^{14} cm^{-2} [18, 19]. Stein [24] and Curtis *et al* [25] observed that electron and hole mobility decreased by less than 5% and 17%, respectively, for a 50% decrease in conductivity due to the neutron irradiation well above 10^{14} cm^{-2}. Thus, equations (2.1) can be written in terms of carrier densities rather than resistivity:

$$N_{mob,e} = N_D \exp\left(-\frac{\Phi}{k_n}\right) \tag{2.3-a}$$

$$N_{mob,h} = N_A \exp\left(-\frac{\Phi}{k_p}\right) \tag{2.3-b}$$

where $N_{mob,e}$ and $N_{mob,h}$ are the mobile carrier densities for n- and p-type silicon, and N_D and N_A are donor and acceptor doping densities.

Assuming that it is applicable everywhere in the semiconductor, the carrier removal is summarized in figures 2.3. The maximum electric field in the region would be reduced by the amount of carriers trapped in the depletion region.

For non-irradiated material, when this maximum electric field reaches the critical electric field E_{crit} (*i.e.*, the electric field that initiates junction breakdown), the applied voltage at the time is [26]

$$V_{BR} \cong \left(\frac{E_{crit}^2 \varepsilon_s}{2q}\right)\left[\frac{N_A + N_D}{N_A N_D}\right] \tag{2.4}$$

where V_{BR} is the breakdown voltage, ε_s is the semiconductor permittivity, q is the coulombic charge, N_A is the doping density at the p-region, and N_D is the doping density at the n-region.

The critical electric field in the depletion region varies slowly with doping density [5]. For a silicon p-n junction where one side is doped much higher than the other, equation (2.4) can be approximated by [5]

$$V_{BR} \cong C \times N_{dop}^{-3/4} \tag{2.5}$$

where C is a constant and N_{dop} is the doping density at highly doped side. Baliga [4] chose C to be 5.34×10^{13} for the parallel-plane structure and suggested equation (1.2).

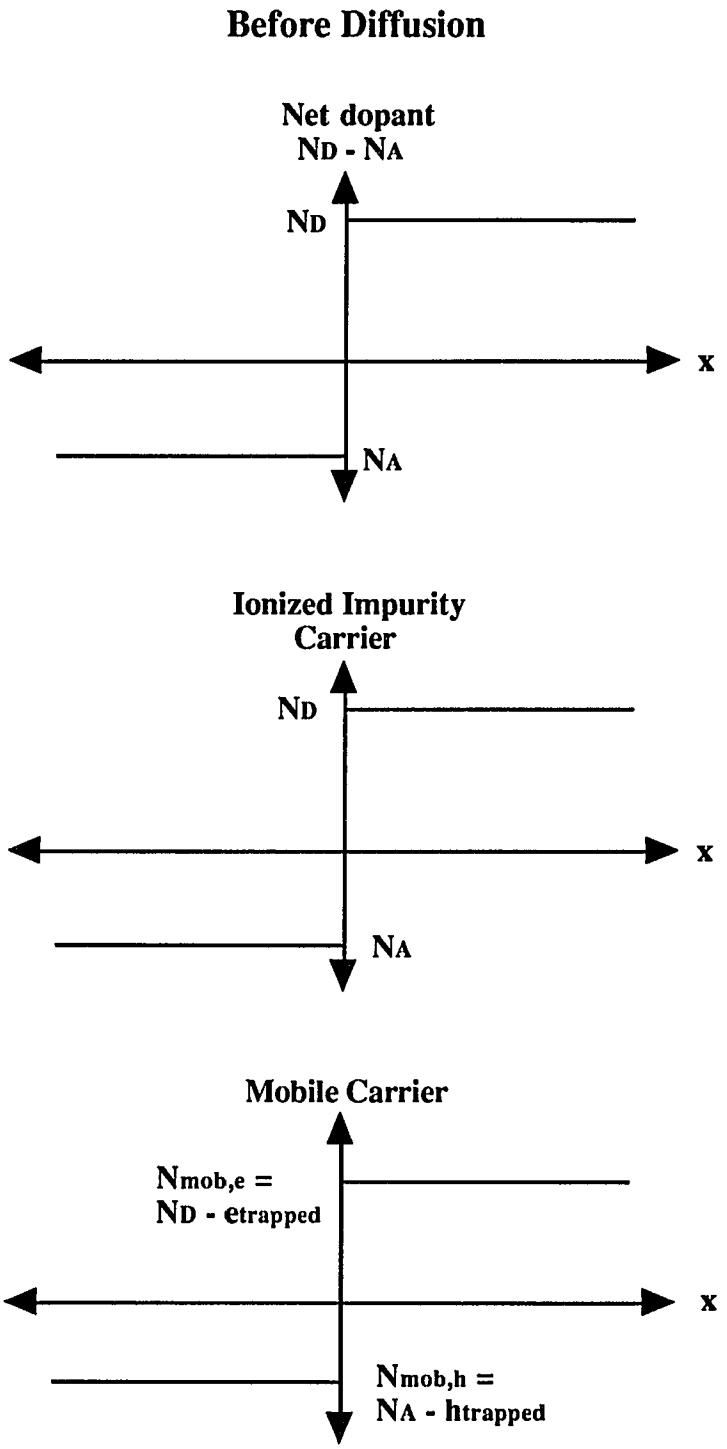

Figure 2.3(a) Creation of mobile carriers in p-n junction before any diffusion due to density gradient taking place

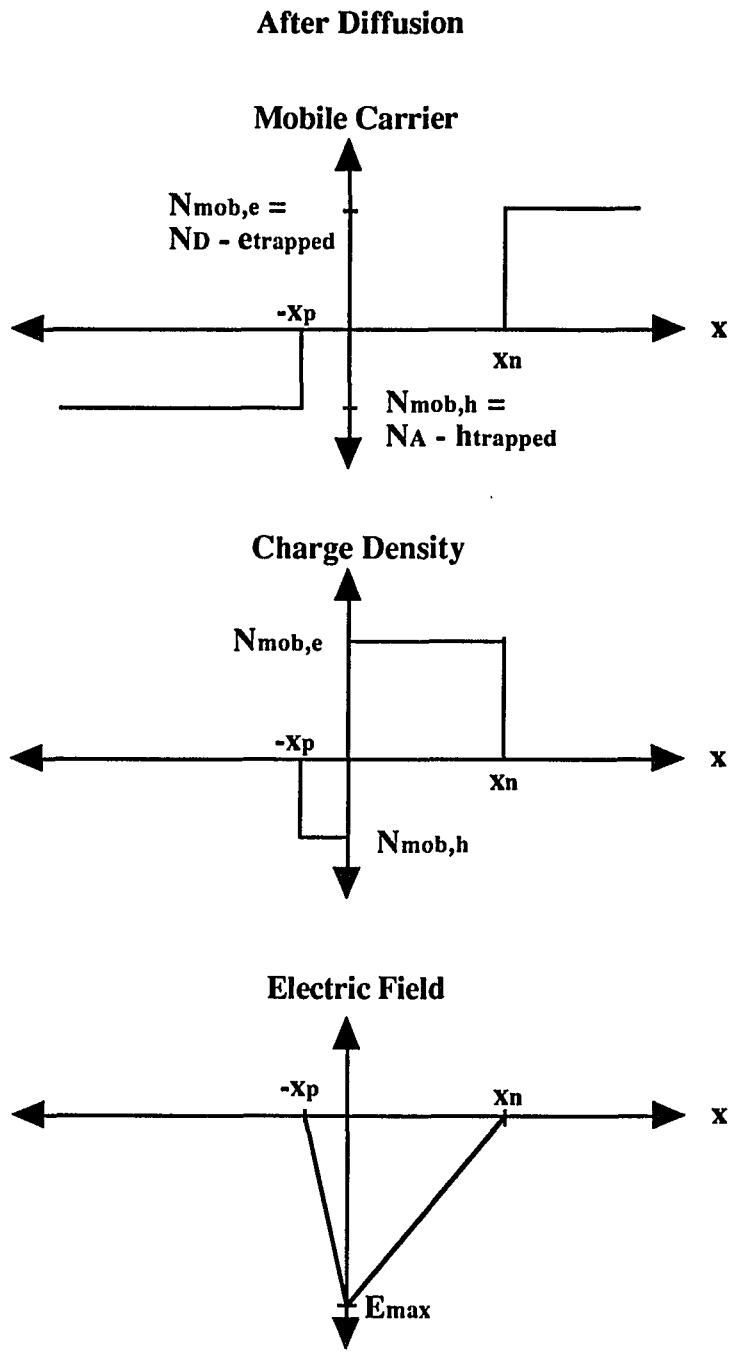

Figure 2.3(b) Application of carrier removal on depleted mobile carrier, charge density and electric field in p-n junction

Combining equation (1.2) and (2.3) give a relation between neutron fluence and the breakdown voltage of power MOSFETs:

$$BV_{pp}(\Phi) = 5.34 \times 10^{13} N_{dop}^{-3/4} \exp\left(\frac{4\Phi}{3k_{n(p)}}\right). \qquad (2.6)$$

Equation (2.6) is derived using the carrier removal model which is a concept of bulk silicon. It will be shown in chapter 5 that this model is not very accurate. When two different types of silicon are brought together, the energy levels bend to give a constant fermi energy throughout the material. This band bending changes the relative positions of defect levels from the fermi energy (see figure 2.4).

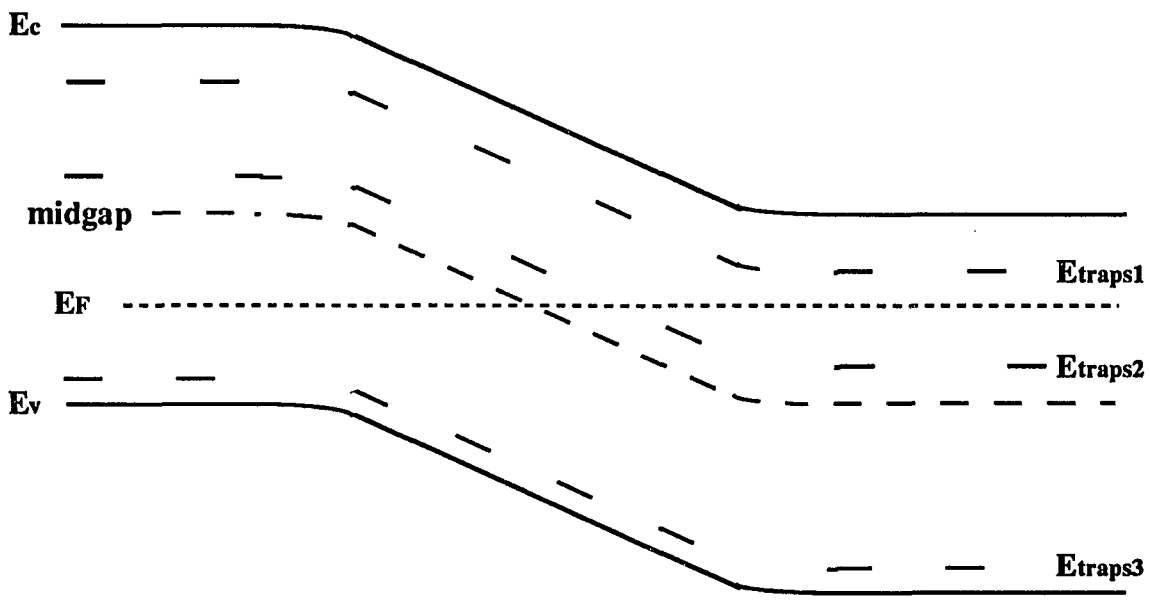

Figure 2.4 Relative position of traps levels to the fermi energy due to the band bending

The effectiveness of a defect in trapping a carrier depends on its relative position to the fermi energy. When the energy bands bend, some traps get closer to the fermi energy, and some other traps get further away. Also, some traps that are above the fermi energy in the neutral region may change to be below the fermi energy, and vice versa, especially traps that are very close to midgap. This situation changes the effectiveness of each defect level to trap carriers depending on its distance from the metallurgical junction.

Figures 2.3 have assumed that traps remove carriers everywhere with the same rate. Actually, $N_{mob,e}$ and $N_{mob,h}$ are functions of distance from the metallurgical junction. Thus, equations (2.3) have to be modified taking into account the effectiveness of defects inside the depletion region as a function of distance from the metallurgical junction. It will be shown that this approach is not practical.

There are at least 29 different kind of defects with energy levels between the valence band E_v and the conduction band E_c. The creation rate of each defect level is unknown and the exact positions of some defect levels are also unknown. Some defects have several energy levels and charge states. For instance, an isolated vacancy has three energy levels and four different charge states. The number of electrons trapped by a vacancy depends on the position of the fermi energy (see figure 2.5) [18]. If the fermi energy is between E_v and E_v+0.05 eV, a vacancy has a positive charge state. The radiation-induced energy level V^+ of the vacancy is located at E_v+0.05 eV. If the fermi energy is above E_v+0.05 eV, the V^+ state is filled by an electron. Likewise, the V^0 state will be filled by an electron if the fermi energy is above E_c-0.4 eV. The position of the last level (V^-) is not exactly known. Depending on how many of its traps are filled, a vacancy can change state to neutral,

negative, or double negative. In a p-n junction, the charge states of vacancies depend on the distance from the metallurgical junction. In a p^+n junction, their charges will vary from negative to neutral. While in an n^+p junction, the charges will vary from neutral to negative and possibly to double negative. This difference is due to the asymmetry of fermi energy position when one side is doped much higher than the other.

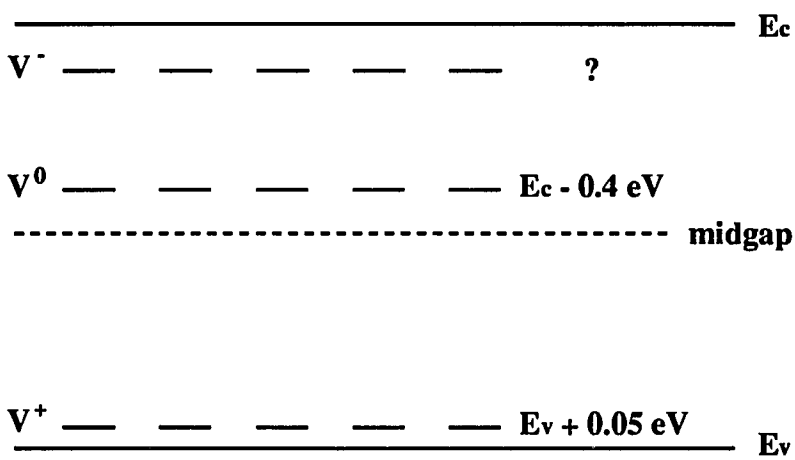

Figure 2.5 Possible energy levels of an isolated vacancy

Vacancies are only one type of the neutron-irradiation-induced defects. It is the most simple and the most understood, but still one of its energy level is not known. There are other defects. Most of them are much more complex and much less understood. To consider and modify equations (2.3) for better accuracy inside the depletion region is impractical.

2.1.2 Change in Mean Free Path

A more practical approach to the change in the breakdown voltage due to the neutron irradiation will be attempted in this sub-section (*i.e.*, by means of the change in mean free path).

Equation (1.4) suggests that avalanche multiplication depends on the mean free path of carriers inside the depletion region. Shockley [12] suggested that, in a non-irradiated p-n junction, only the mean free path due to scattering from Raman phonons is important.

Carriers in a crystal experience random collisions due to scattering centers. An important characteristic of a scattering center is its cross section. If a carrier experiences c collisions due to one type of scattering center per unit distance travel, while there are N such scattering centers per unit volume, the collision cross section is

$$\sigma = \frac{c}{N} \tag{2.4}$$

The average distance (also called collision mean free path) traveled by the carriers is

$$L = \frac{1}{c} \tag{2.5}$$

If there is more than one kind of scattering center, each causing c_i collisions per unit distance traveled, then the total number of collisions per unit distance traveled is

$$c_t = \Sigma c_i \tag{2.6}$$

or

$$\frac{1}{L_t} = \Sigma \frac{1}{L_i} = \Sigma \frac{1}{\sigma_i N_i} \tag{2.7}$$

Charge transport in semiconductors involves four important scattering mechanisms: phonon, defect, impact ionization, and carrier-carrier scattering [27]. When the number of lattice dislocations is negligible, only phonon scattering and impact ionization are important in the depletion region. As the number of dislocations increases, the collision mean free path is reduced.

Equation (2.7) suggests that the collision mean free path decreases as the number of the defects increases. Equation (1.4) suggests that the b coefficient of Chynoweth's law increases, and the impact ionization rate decreases. The decrease of the impact ionization rate increases the breakdown voltage since a higher electric field is needed in the depletion region to produce the same avalanche multiplication.

2.2 Ionizing Radiation Damage

Neutron testing in a nuclear reactor is always accompanied by a certain amount of gamma radiation. The concomitant gamma radiation from a neutron irradiation source possesses enough energy to break atomic bonds and create electron-hole pairs in the oxide of the MOSFET structure. Since electrons have higher mobility and a lower trapping rate than holes, positive trapped-charges are dominant in bulk SiO_2 after gamma irradiation [28]. Positive oxide charge changes the equipotential lines, as shown in figure 1.6. It also shifts the MOSFET threshold voltage to a more negative value [28].

CHAPTER 3

EXPERIMENTAL PROCEDURE AND RESULTS

Six types of n-channel and four types of p-channel DMOS power transistors with various breakdown voltage ratings were exposed to neutron irradiation. The ten transistors used are listed in table 3.1.

Model Number	Type	Rating	Measured BV
MTM12N10	n-type	100 V	117.0 V
MTM10N25	n-type	250 V	314.5 V
MTM10N25	n-type	250 V	310.7 V
2N6759	n-type	350 V	427 V
IRF440	n-type	500 V	561 V
IRF440	n-type	500 V	551 V
MTM8P10	p-type	100 V	114.3 V
MTM2P45	p-type	450 V	569 V
MTM2P50	p-type	500 V	551 V
MTM2P50	p-type	500 V	552 V

Table 3.1. DMOS transistor breakdown voltage ratings

Sources, drains, and gates of the transistors were tied together, giving zero bias conditions during the irradiation. The transistors were characterized at total neutron fluences of 10^{11}, 10^{12}, 10^{13}, $5x10^{13}$, 10^{14}, and $5x10^{14}$ neutron/cm^2. The characterization

after radiation exposure had to wait about half an hour for safety purposes, due to residual radiation of the transistors. A Ni foil dosimeter was used for each fluence level. The neutron radiation counts were calibrated using results from the National Institute of Standards and Technology.

To see the effect of the concomitant gamma radiation on the device breakdown voltage, four transistors were irradiated in a Cobalt-60 source. Two of each n-channel and p-channel device type with breakdown voltages of 100 and 500 V were used. The neutron irradiation source produces approximately 11 rads(Si)/kW*s of gamma radiation. The four transistors were irradiated and characterized at approximately 170 rads(Si), 1.7 krads(Si), 16.8 krads(Si), 84 krads(Si), 171 krads(Si), and 884 krads(Si) to allow comparison with concomitant gamma radiation at neutron fluences of 10^{11}, 10^{12}, 10^{13}, $5x10^{13}$, 10^{14}, and $5x10^{14}$ neutron/cm^2.

3.1 Breakdown Voltage Measurement

Breakdown voltages of the MOSFETs were measured using the circuit shown in figure 3.1. A fuse and a resistor were used for protection. A customized test fixture was made to minimize human interaction with the device under test. This test fixture and the circuit in figure 3.1 were compared with a commercially available HP 16058A test fixture using an HP 4145B Semiconductor Parameter Analyzer. The results for 100 V n- and p-type MOSFETs are shown in figures 3.2 and 3.3. The customized test fixture and the commercial test fixture show comparable results.

The breakdown voltage was defined as the voltage when a current of 1 mA flowed while the channel region of the device was off. This definition is sufficiently accurate since the slopes of the I-V curves are very sharp, as shown in figures 3.2(a) and 3.3(a).

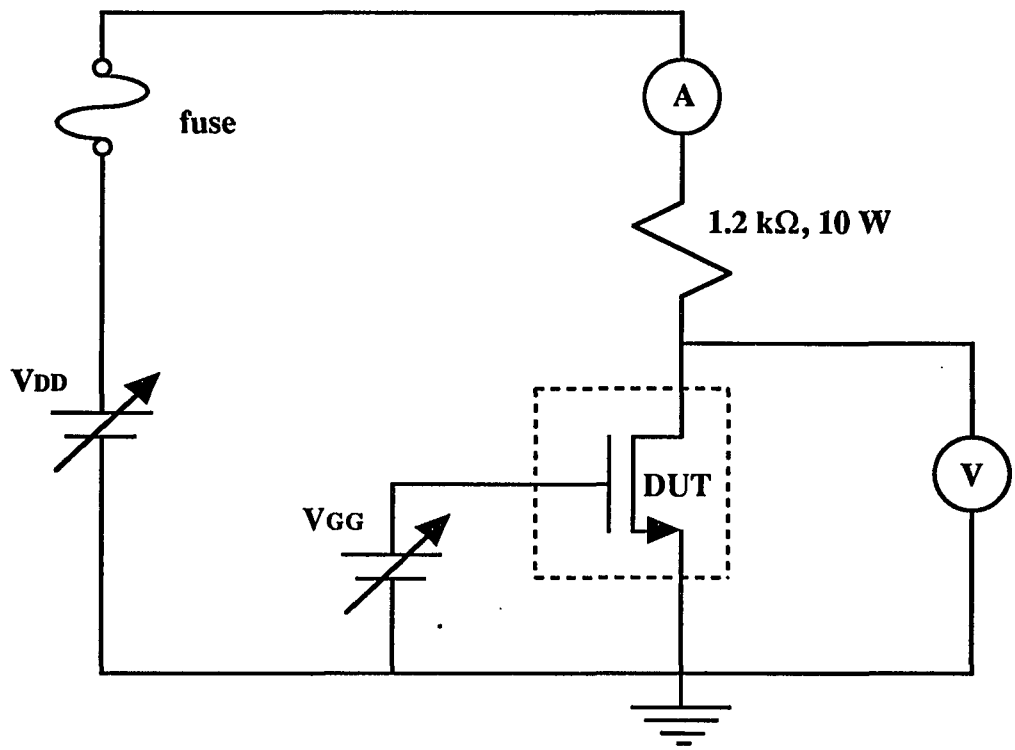

Figure 3.1 Circuit to measure breakdown voltage

All the MOSFETs used are enhancement type (normally off). However, the positive oxide charges trapped during irradiation could form a channel, making the n-type transistors become depletion mode. Thus, it is necessary to have a negative gate bias to keep the device turned off in case this happens. The threshold voltages of the devices after each irradiation were measured using an HP 4145B Semiconductor Parameter Analyzer in the configuration shown in figure 3.4. Shielding is needed to protect the experimenter from any residual radiation left in the transistors.

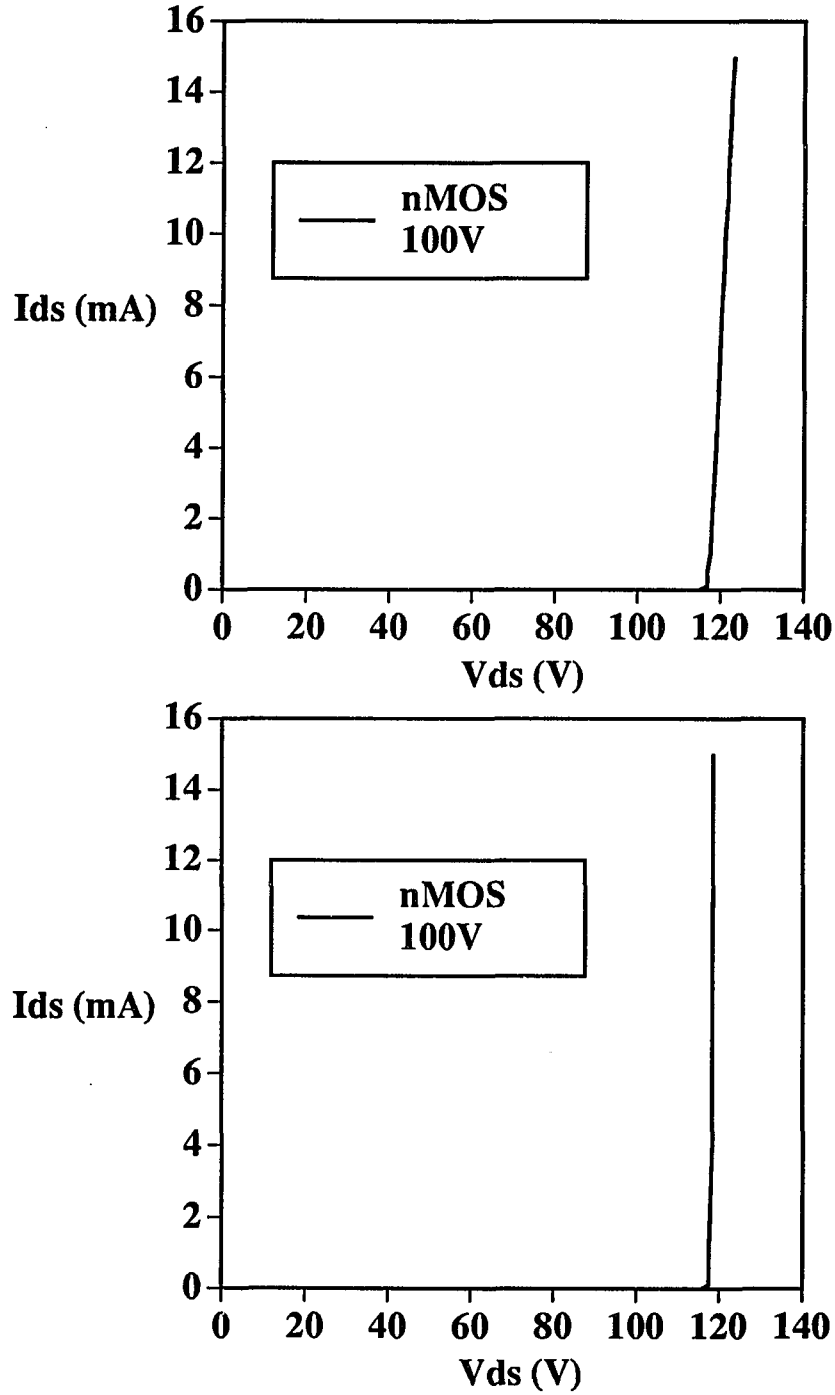

Figure 3.2 Breakdown voltage measurement comparison for a 100-volt nMOSFET: (a) using custom test fixture (b) using commercially available test fixture

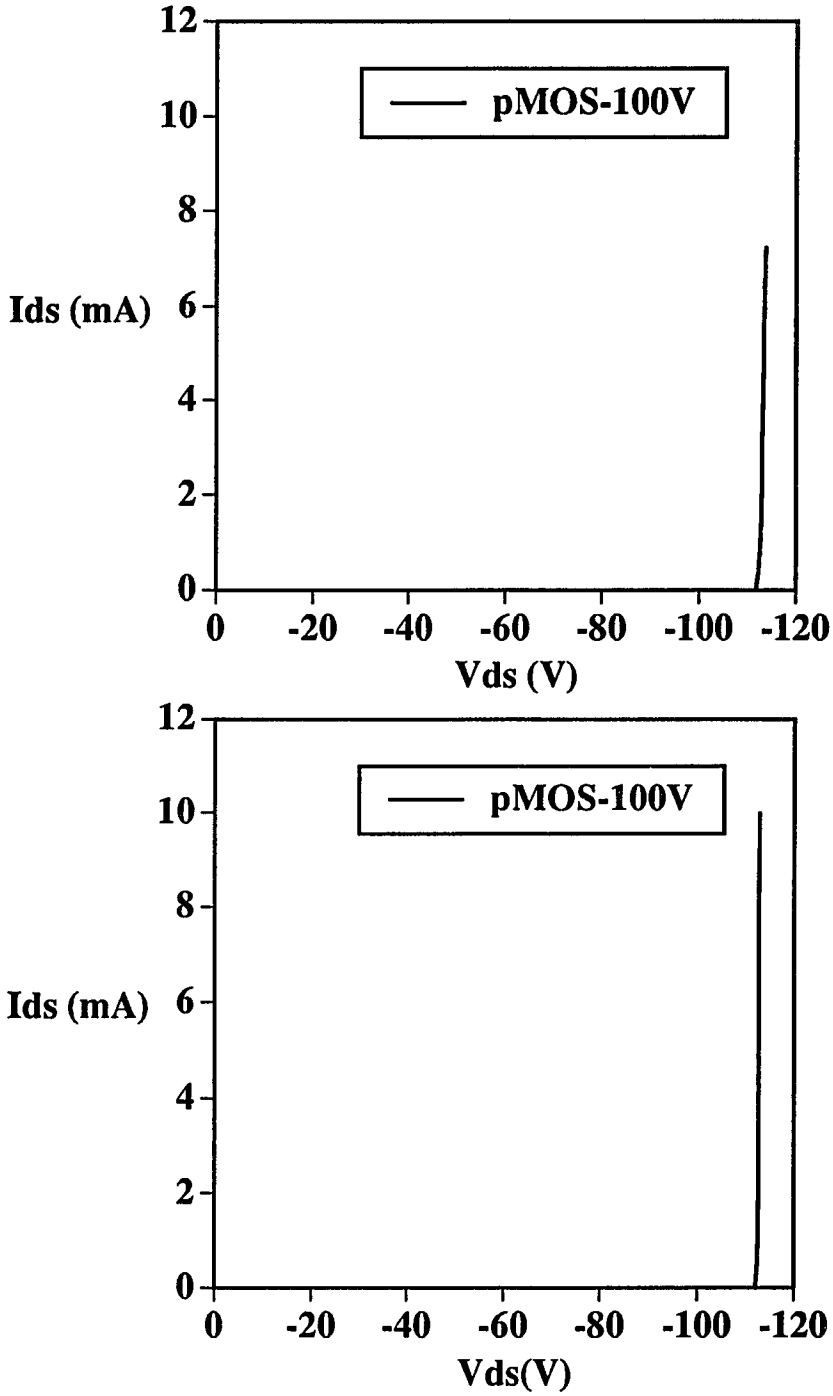

Figure 3.3 Breakdown voltage measurement comparison for a 100-volt pMOSFET: (a) using custom test fixture (b) using commercially available test fixture

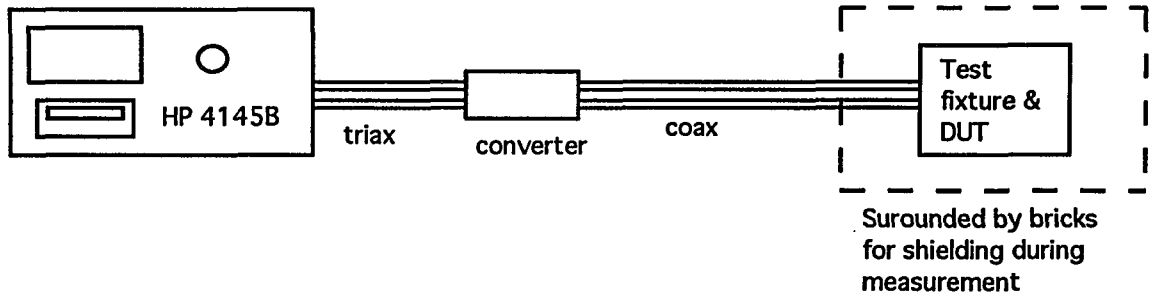

Figure 3.4 Threshold voltage measurement

3.2 Radiation Source

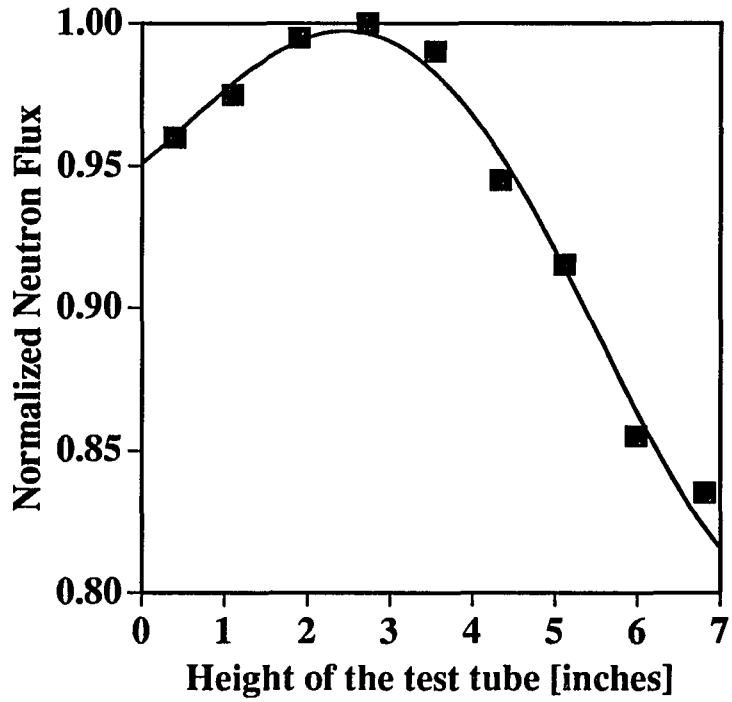

Figure 3.5 Normalized neutron flux profile of FIR facility

Neutron irradiation was performed at the University of Arizona's research reactor facility. The reactor is a TRIGA swimming pool-type with neutron flux in fast irradiation (FIR) facility of approximately 6.9 x 10^9 neutron/cm^2-sec-kW (E > 10 keV). The neutron flux profile as a function of height from the bottom of the test tube is shown in figure 3.5. The concomitant gamma dose rate in FIR is approximately 11 rads(Si)/sec-kW and its flux profile is shown in figure 3.6.

Gamma radiation was performed in the Co^{60} radiation facility of the University of Arizona.

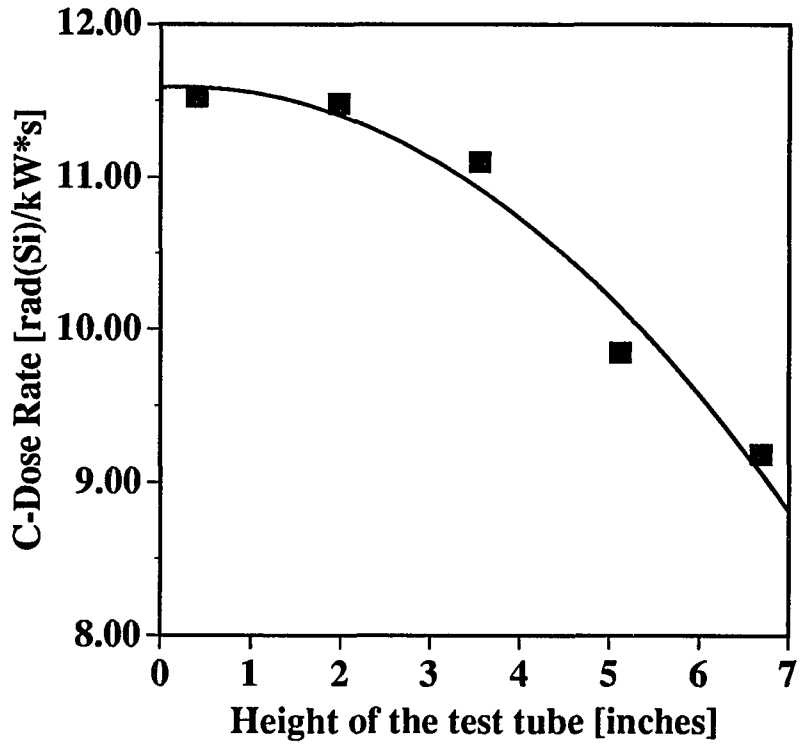

Figure 3.6 Concomitant gamma dose rate of FIR facility

3.3 Results

3.3.1 Results of the Neutron Irradiation Experiments

Figures 3.7 and 3.8 show the change in the breakdown voltages of the n- and p-type MOSFETs as a function of neutron fluence. Figure 3.7 shows that all the n-type MOSFETs experience very small decreases in their breakdown voltages after neutron fluences up to the 10^{13} cm^{-2}. Then their breakdown voltages start to increase. Above 10^{13} cm^{-2}, the increase in breakdown voltage is noticeable, especially for the higher rated transistors. With the exception of the 500-volt devices, the transistors show a tendency that the higher the voltage rating, the bigger the change at a particular fluence level.

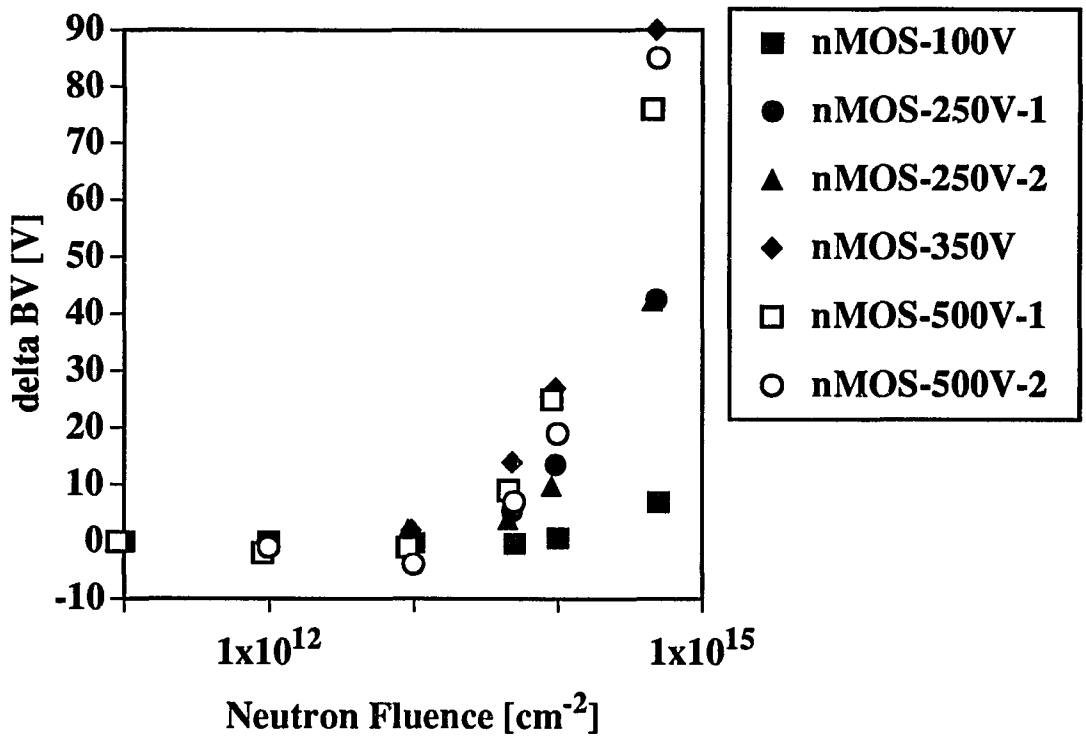

Figure 3.7 Change of breakdown voltage of n-MOSFETs due to neutron irradiation

Figure 3.8 shows that relatively small changes happen to p-MOSFETs after neutron fluences up to 10^{12} cm^{-2}. One of the 500-volt devices experiences about 10V decrease in its breakdown voltage, while the other one only experiences about 1V decrease. The breakdown voltage of the 100-volt device is relatively unchanged. Above 10^{12} cm^{-2} and up to 10^{14} cm^{-2}, all devices experience an increase in their breakdown voltages. The increase in the breakdown voltages is relatively faster than that experienced by the n-type MOSFETs. Above 10^{14} cm^{-2}, anomalies happen to the higher-rated p-MOSFETs. The increase in breakdown voltage saturates and then starts to decrease. The 100-volt device breakdown voltage continues to increase up to the maximum fluence in the experiment.

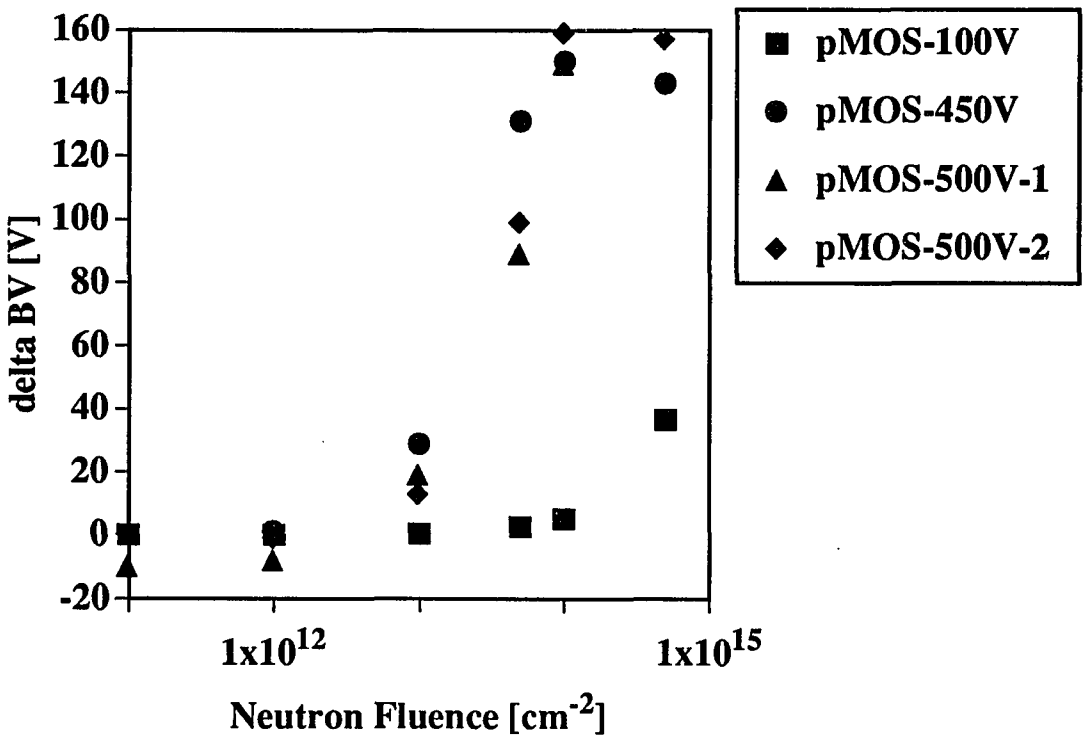

Figure 3.8 Change of breakdown voltage of p-MOSFETs due to neutron irradiation

3.3.2 Results of the Gamma Irradiation Experiments

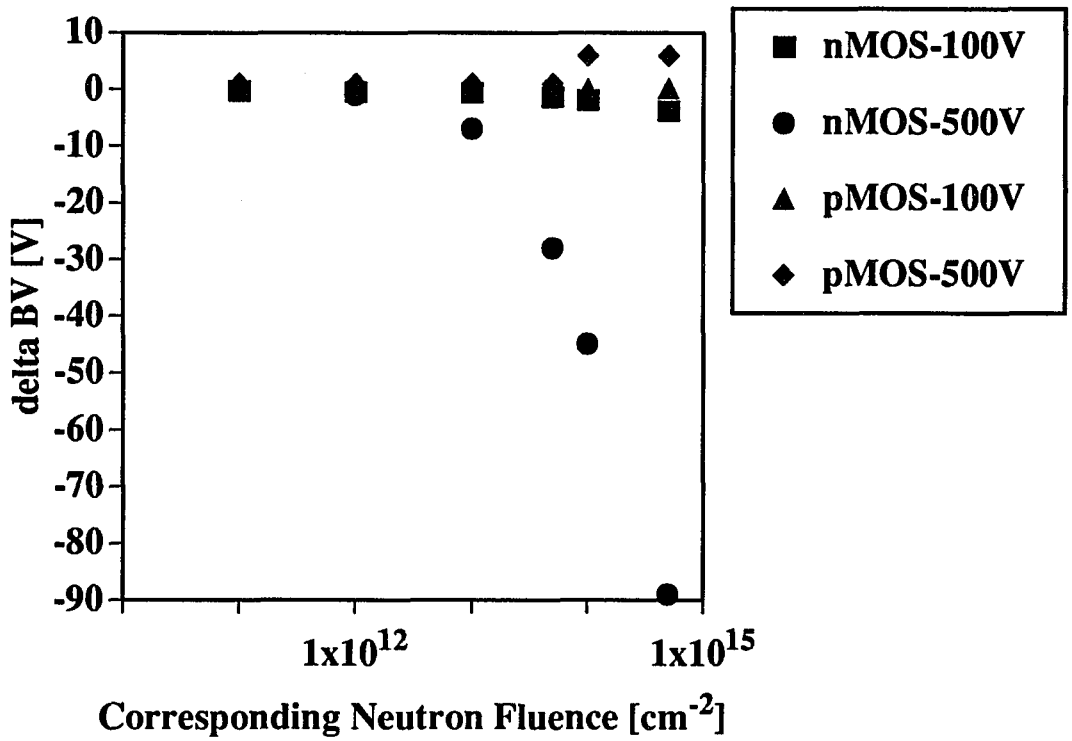

Figure 3.9 The effect of concomitant gamma radiation to the change of the breakdown voltage of n- and p-MOSFETs

The effect of gamma radiation on the breakdown voltages of n- and p-type MOSFETs is shown in figure 3.9. Two of each type were irradiated. They represent the highest and the lowest rating of the n- and p-type MOSFETs used in the neutron irradiation experiments. Small positive changes to the breakdown voltage happen to both p-type devices for all levels of gamma radiation corresponding to the fluences of the neutron irradiation experiments. A small decrease in the breakdown voltage happens to the 100-volt n-type MOSFET.

Considerable decrease in the breakdown voltage of the 500-volt n-type device occurs, especially after gamma radiation corresponding to the neutron fluences above 10^{13} cm^{-2}. The changes below 10^{13} cm^{-2} are consistent to what happens to the same devices in neutron irradiation experiments. Above 10^{13} cm^{-2}, opposite effects happen in gamma and neutron irradiation experiments.

CHAPTER 4

S-PISCES 2B SIMULATION

S-PISCES 2B device simulation was used to simulate the effect of the change in mean free path on the breakdown voltage of the power MOSFETs. This effect was introduced by adjusting the ionization coefficients of Chynoweth's law, specifically by changing the b coefficient according to equation (1.4).

Breakdown voltage simulation using S-PISCES 2B can be divided into roughly three stages: grid generation to define the device structure, application of step voltages until breakdown is reached, and generating the desired output, such as the I-V characteristic of the device. The number of arithmetic calculations to achieve solution for each step voltage is almost squarely proportional to the number of grid points [29]. Also, there is a maximum number of nodes that can be handled. For the two-carrier, full Newton method used in these breakdown voltage simulations, the maximum number of nodes is 4,800 [29].

Simulation time is proportional to the number of arithmetic calculations and the number of voltage steps. Device structures with many field rings require many fine grids. High voltage simulations of power devices require many voltage steps. These conditions mean that breakdown voltage simulation of power devices with multiple rings will require days of CPU time. To avoid lengthy simulation, device simulations in this work were limited to one-dimensional structures. Figure 4.1 shows a p-n junction structure for a 100-

volt n-type device. The junction is basically the body-to-drain junction. Figure 4.2 shows the diffusion profile of the 1-d structure in figure 4.1.

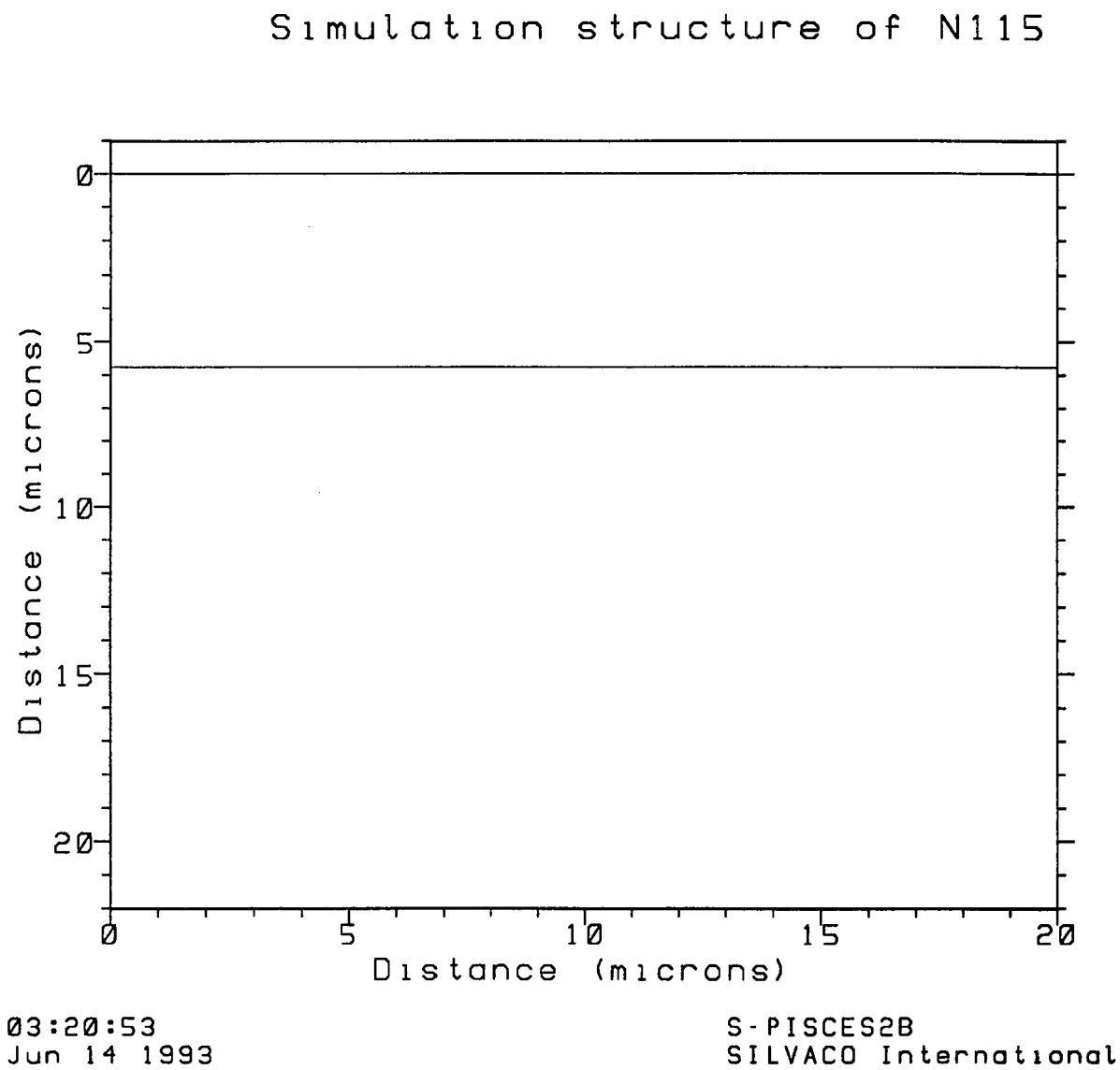

Figure 4.1 One dimensional structure

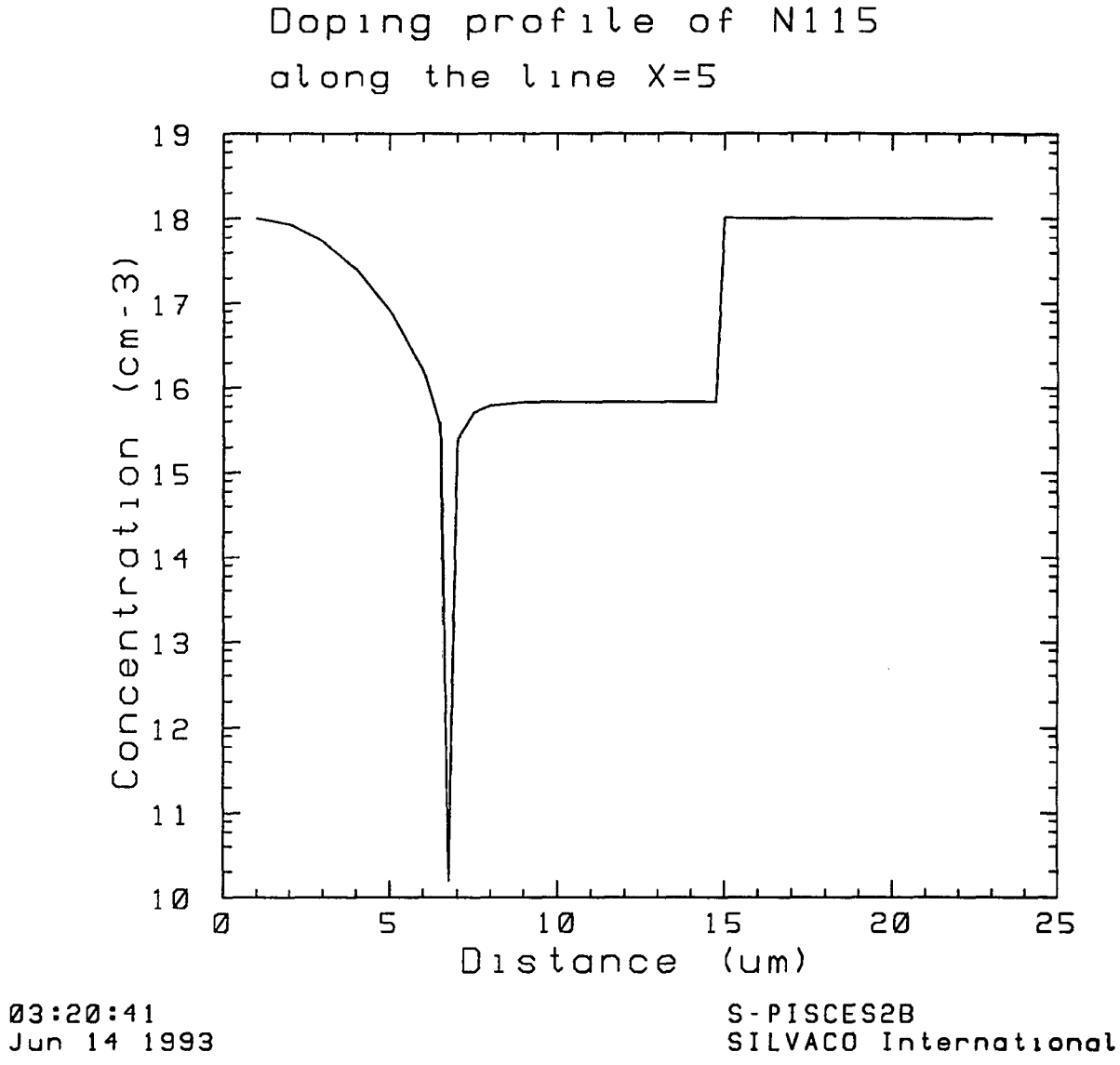

Figure 4.2 Diffusion profile of the 1-d diode structure

Some data, such as device structure, drain to body junction depth, epi-layer thickness, and epi-layer doping density are needed to construct the simulation structure. Since the manufacturer could not provide this information, destructive tests to the devices were performed to obtain reasonable values.

The tests provided dimensional variables such as drain to body junction depths, epitaxial thickness, and termination structure type. Up to seven floating guard rings were observed on the devices. Using many rings is a way to approach the ideal-parallel-plane breakdown voltage values. Properly terminated devices may reach as high as 90% of their ideal breakdown voltages [14, 15].

Important parameters and initial breakdown voltages obtained from simulation are listed in table 4.1. The values for N_{epi} in the table were selected to provide breakdown voltages very close to those of the actual devices. The first approximation of the doping density for each device is obtained from equation (1.2). The doping densities were then refined recursively using the results from previous simulations until the simulated breakdown voltages were within approximately 1% of the measured breakdown voltages of the actual devices. The doping densities of the highly doped side of the junction were made at least 100 times N_{epi}.

Rating	Type	x_j	W_{epi}	N_{epi} (cm^{-3})	BV_{meas}	BV_{sim}
100 V	n-type	5.75 μm	14.00 μm	6.80 E15	117.0 V	116 V
250 V	n-type	5.00 μm	26.50 μm	1.11 E15	314.5 V	315 V
500 V	n-type	4.00 μm	43.86 μm	4.70 E14	551 V	550 V
100 V	p-type	6.29 μm	14.06 μm	7.10 E15	114.3 V	113 V
500 V	p-type	5.86 μm	40.51 μm	5.10 E14	552 V	552 V

Table 4.1. Device simulation parameters and their breakdown voltages

S-PISCES 2B provides several models of impact ionization [29]. The Selberherr model was chosen, because it is readily modified to Chynoweth's law of equation (1.3). Selberherr's formula follows the generation rate of equation (1.1) and $\alpha_{n(p)}$ is determined by [30]

$$\alpha_{n(p)} = a_{n(p)} \exp\left[-\left(\frac{b_{n(p)}}{E}\right)^{\beta_{n(p)}}\right] \tag{4.1}$$

where $\beta_{n(p)}$ is a constant ranging from 1 to 2 for electrons (holes). Keeping this constant equal to 1 makes Selberherr's formula identical to Chynoweth's law. Along with this formula, the ionization coefficients of Van Overstraeten and De Man were used.

The ionization coefficients of Van Overstaeten and De Man are divided into two regions with the boundary between the high and the low field regions located at 4.0×10^5 V/cm. Coefficients for electrons are the same for both regions, while the hole coefficients are different. Figure 4.3 shows the hole ionization coefficients with the boundary between the two regions called E_{gran}.

E_{gran} is established by equating the ionization-coefficient curves in both regions. Introduction of the neutron-irradiation effect will increase the slopes of the curves and this will make the two curves discontinuous at E_{gran}. To avoid this discontinuity after changing the b coefficient, the low and high field equations are equated giving a new boundary at E'_{gran}. The new boundary electric field is

$$E'_{gran} = \left(\frac{b'_{p2} - b'_{p1}}{\ln\left(a'_{p2}/a'_{p1}\right)}\right) \tag{4.2}$$

where the subscript 1 is for the high field region and the subscript 2 is for the low field region.

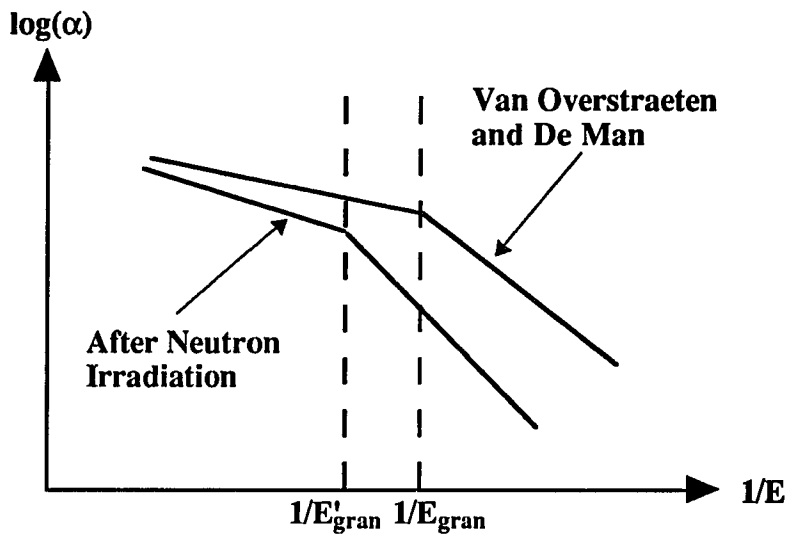

Figure 4.3 Effect of neutron irradiation on the hole ionization rate

No data are available for electron or hole scattering due to defects in the presence of a high electric field, so a strategy for the simulation has to be developed. Simulations will be done by changing the b coefficient arbitrarily. After a few results are obtained, the relation between the change in the b coefficients and the change in breakdown voltage will be observed.

Results of the simulations are shown in table 4.2. The table shows the change in b coefficients and breakdown voltage. A linear increase is observed for each device.

Rating	Type	b(Φ)/b(0)	BV_{sim}
100 V	n-type	1.00	116 V
		1.02	120 V
		1.04	124 V
250 V	n-type	1.00	315 V
		1.04	336 V
		1.06	346 V
		1.08	357 V
500 V	n-type	1.00	550 V
		1.04	588 V
		1.08	627 V
		1.09	637 V
100 V	p-type	1.00	113 V
		1.04	120 V
		1.17	145 V
		1.20	151 V
		1.22	154 V
500 V	p-type	1.00	552 V
		1.05	598 V
		1.17	707 V
		1.20	734 V
		1.23	761 V

Table 4.2. Change in b coefficient and breakdown voltage

From the data in table 4.2, the normalized values of the breakdown voltage are plotted versus the normalized value of the b coefficient in figure 4.4. It shows a linear relationship with a slope S of approximately 1.724. So

$$S = \left(\frac{\Delta BV}{BV_{PP}}\right) \Big/ \left(\frac{\Delta b}{b(0)}\right) = 1.724. \qquad (4.2)$$

This empirical constant will be useful in deriving the ionization coefficients as a function of neutron fluence, once a breakdown voltage model as a function of neutron fluence is developed. The ionization coefficients model will help device simulations in the future.

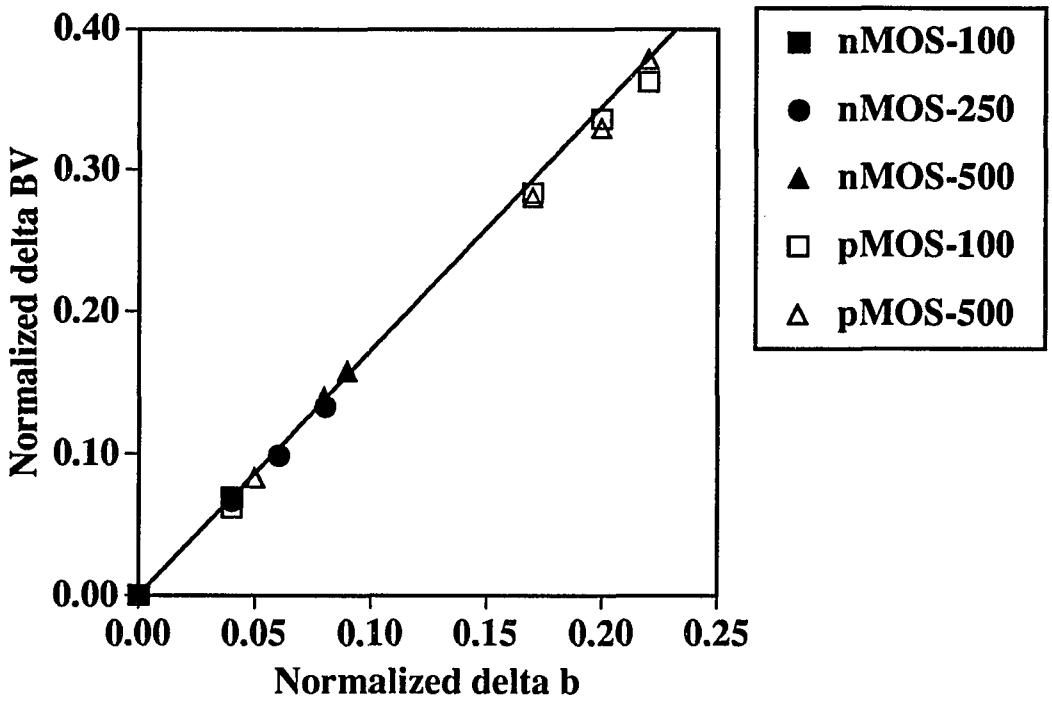

Figure 4.4 Normalized plot of the change in breakdown voltage and the change in b coefficient

For comparison purposes, table 4.3 shows breakdown voltages for some devices after a fluence of $5x10^{14}$ cm^{-2} and the corresponding change in b coefficients needed for the devices to have such breakdown voltages. The table shows as little as 4% change in the b coefficients gives the necessary breakdown voltage change experienced by a 100-volt

nMOSFET after neutron irradiation of $5x10^{14}$ cm^{-2}. The table also shows that the change in the normalized b coefficient for n- and p-type MOSFETs that is required to make the simulations agree with the experiment differs by a factor between approximately 2 and 5. This will be explained in the next chapter.

Rating	Type	Φ	BV(Φ)	b(Φ)/b(0)	BV_{sim}
100 V	n-type	$5x10^{14}$ cm^{-2}	123.9 V	1.04	124 V
250 V	n-type	$5x10^{14}$ cm^{-2}	357 V, 353 V	1.08	357 V
500 V	n-type	$5x10^{14}$ cm^{-2}	637 V, 636 V	1.09	637 V
100 V	p-type	$5x10^{14}$ cm^{-2}	150.8 V	1.20	151 V
500 V	p-type	$5x10^{14}$ cm^{-2}	700 V, 711 V	1.20	734 V

Table 4.3. Change in b coefficient correspond to the $5x10^{14}$ cm^{-2} of neutron irradiation

CHAPTER 5

DISCUSSION

Power MOSFETs with various breakdown voltage ratings were irradiated with neutrons. The effects of the radiation on the breakdown voltage of the devices were investigated. Two kinds of radiation need to be considered: neutron irradiation that causes dislocations and concomitant gamma radiation that produces positive oxide charge.

5.1 Gamma Radiation

To distinguish the effect of the neutron effects from the concomitant gamma radiation, gamma radiation exposures using a Co60 radiation facility were performed. With the exception of the 500V NMOS devices, all results show very small changes due to gamma irradiation. However, the results show that n-type MOSFETs exhibit a decrease in breakdown voltage values while the p-type MOSFET breakdown voltages increase. This is consistent with the investigations of Kosier *et al* [17].

Positive oxide charges are created by the gamma radiation. This charge disturbs the equipotential lines in the depletion region close to the Si-SiO_2 interface. The change in equipotential lines decreases the breakdown voltages of the n-type power MOSFETs. In the p-MOSFETs, small amounts of positive oxide charge increase the breakdown voltages.

However, a large amount of positive oxide charge may or may not enhance the breakdown voltages. It may actually decrease them [17].

5.2 Low Neutron Fluence

At low neutron fluence levels (up to 10^{13} cm^{-2} for n-type and up to 10^{12} cm^{-2} for p-type MOSFETs), only small changes in breakdown voltage are observed. All NMOS transistors show small increases in their breakdown voltage values. Some PMOS transistors decrease and others increase. It is believed that a relatively small number of dislocations occur at this low fluence level. This small number of dislocations should affect the scattering mean free path L and the ionization rate α insignificantly.

Since the scattering mean free path L changes insignificantly, the breakdown voltage changes in this low neutron fluence should be due to the concomitant gamma radiation. The gamma irradiation experiments, with the amount of gamma radiation equal to the concomitant doses encountered at in the neutron experiments, show small changes in the breakdown voltages of all four transistors (see figure 3.9). Small decreases are observed in the breakdown voltages of the n-type MOSFETs (up to a corresponding neutron fluence of 10^{13} cm^{-2}) and practically no changes are observed in the breakdown voltages of the p-type MOSFETs (up to a corresponding neutron fluence of 10^{12} cm^{-2}). In the neutron irradiation experiment, all n-type MOSFETs first experience small decreases in their breakdown voltages. As the fluence level approaches 10^{13} cm^{-2}, most n-type devices still have lower breakdown voltages than their initial values, but some have shown

recovery and increases. The latter obviously have already encountered some effects from the change in the mean free path due to the atomic dislocations.

P-type devices in the low-fluence neutron irradiation experiment show some interesting results. The 100-volt device has its breakdown voltage relatively unchanged, but the 500-volt devices have some decreases in their breakdown voltages. The decrease in one of these 500-volt devices is as much as 10 V, while the other is merely 1 V.

In the p-MOSFETs, small amounts of positive oxide charge increase the breakdown voltages. However, a large amount of positive oxide charge may or may not enhance the breakdown voltages, and may actually decrease them [17]. Kosier *et al* considered uniform positive charge distribution in the oxide due to the gamma radiation. In neutron radiation, some dislocations occur in the oxide. These dislocations could disturb the uniformity of the oxide charge near the Si-SiO_2 interface. This non-uniformity makes higher positive charge densities at some locations and lower densities at some other places. Localized higher positive charge densities can decrease the breakdown voltage of a p-type MOSFET instead of increasing it.

In short, a low-level neutron fluence is a fluence where the atomic dislocations due to the neutron radiation are not yet dominant. Combination of the effect of the small change in the ionization rate, the effect of the change in the equipotential lines, and the enhanced effect of localized higher densities of positive oxide charge have produced the observed effect in the low neutron fluence region.

5.3 High Neutron Fluence

All transistors show breakdown voltage increses in the high neutron fluence region (above 10^{13} cm^{-2} for n-type and above 10^{12} cm^{-2} for p-type MOSFETs). The change in this region is believed to be primarily due to the change of the collision mean free path.

Dislocations introduce new scattering centers throughout the material. These new scattering centers have a total collision mean free path L_D. In the low fluence region, L_D is still much larger than the Raman phonon mean free path L_R, so the total value of the mean free path L_T is still approximately L_R according to equation (2.4). In this high fluence region, though still larger than L_R, L_D starts to affect the total mean free path L_T considerably.

Device simulations have been done for this region. The effect of atomic dislocations can be described by using a larger b coefficient in Chynoweth's law (see equation (1.4)). Assuming no change in ionization energy, as little as 4% change in L_t gives the necessary breakdown voltage change experienced by a 100-volt nMOSFET after a neutron fluence of $5x10^{14}$ cm^{-2} (see data in table 4.2).

The change in the mean free path ΔL_T for n- and p-type power MOSFETs that is required to make the simulations agree with high-neutron-fluence experiment differs by a factor between 2 and 5. This relatively high difference could possibly be due to the difference in total cross section of the defects in the n- and p-type material. (A five-times bigger cross section translates to a five-times smaller mean free path.) This big difference is not unlikely to occur, considering that there are at least 29 different kind of defects that

depend on the material, doping, and energy transfer during the irradiation. Stein [24] and Curtis *et al* [25] had observed a difference of more than a factor of three in the decrease of the electron and hole mobilities due to the neutron radiation. Though this is not exactly the same mechanism, it suggests that a large difference between responses of n- and p-type material is reasonable.

5.4 Device Limiting Factor

For most devices in this experiment, the upward trend of $\Delta BV(\Phi)$ continues to the highest fluences examined. However, figure 3.8 shows that the breakdown voltages of the high-voltage p-type MOSFETs saturate, although the cumulative neutron fluence increases. Also, in figures 5.1, it is shown that the rate of increase in the breakdown voltage of the high-voltage n-type MOSFETs has slowed down. Figure 5.1(a) is in logarithmic scale, and figure 5.1(b) is in linear scale. Both figures are showing the same curve fit and they show that the point at $5x10^{14}$ cm^{-2} is below the curve fit.

In the high-voltage p-type MOSFETs, the breakdown voltages start to decrease after a fluence of 10^{14} cm^{-2}, with the maximum breakdown voltages a little bit more than 700 V. At 700 V, with N_{epi} approximately $5x10^{14}$ cm^{-3}, the depletion width of these devices would be around 42 μm. The epitaxial layer of these devices is also around 42 μm. With body-to-drain metallurgical junction x_j equal to approximately 6 μm, the lowly doped drain region is approximately 36 μm. This means that the vertical depletion region that could be supported by the p^+nn^+ structure is only about 36 μm. Since, at 700 V, the

depletion region needed is 42 μm, punchthrough of the low doped n region has happened. Figures 5.2 illustrate this condition.

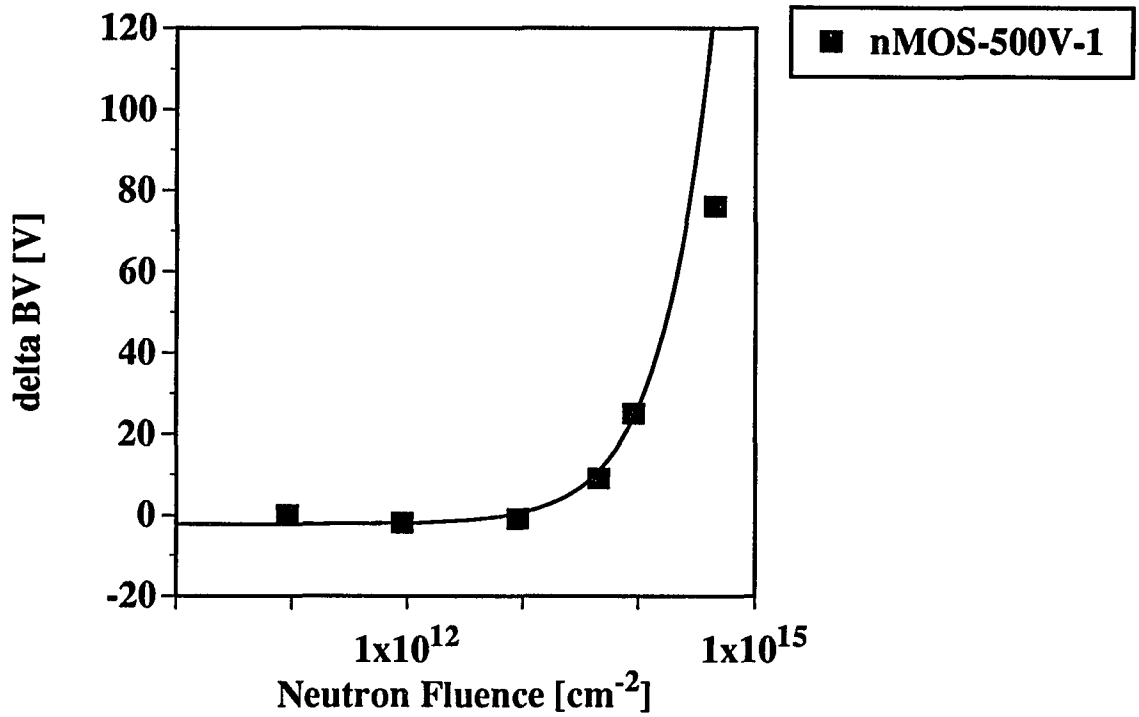

Figure 5.1(a) The change in the breakdown voltage of a 500-volt NMOS device versus neutron fluence: log scale

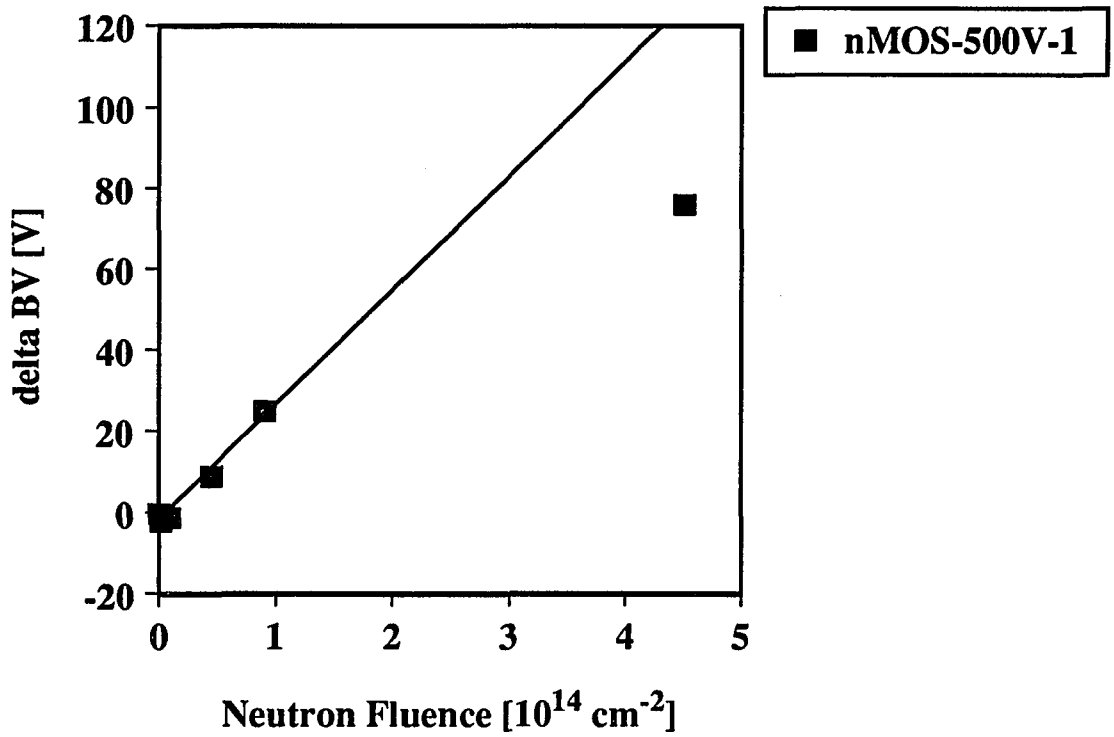

Figure 5.1(b) The change in the breakdown voltage of a 500-volt NMOS device versus neutron fluence: linear scale

Figure 5.2 shows the non-punchthrough and punchthrough conditions in p^+nn^+ diodes. Figure 5.2(a) shows the electric field curve of a p^+nn^+ that has an infinitely long n region (it is basically a p^+n diode). The depletion region gets wider until the junction breaks down. Figure 5.2(b), on the other hand, shows the electric field in the depletion region of a p^+nn^+ diode that has thickness of the n region x_n. Since the p^+ and n^+ regions have much higher doping than the n region, the maximum depletion width that can be supported by the diode is approximately x_n. If the voltage is increased after x_n is reached, instead of reaching x_v, the E versus x curve is shifted up to accommodate the area that

would otherwise appear beyond x_n. This makes the electric field inside the depletion region of this device higher than that of the p^+nn^+ diode with an infinitely long n region. The breakdown of the limited-n-region p^+nn^+ diode happens at a lower voltage. This condition limits the increase of the breakdown voltages due to the neutron radiation.

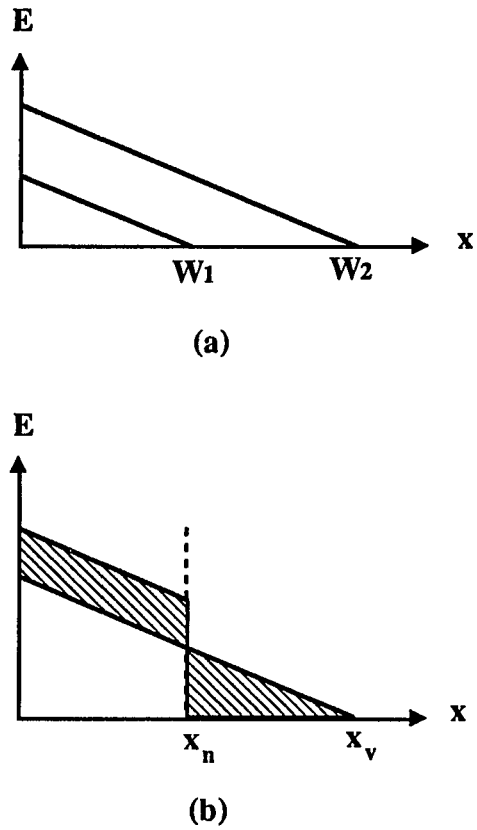

Figure 5.2 Non-punchthrough and punchthrough of p^+nn^+ diode

All devices in this experiment start with a depletion region at breakdown thinner than their lowly-doped drain region. High-fluence neutron irradiation increases breakdown voltages of the devices. The 500-volt and the 450-volt devices eventually have breakdown

voltages that make the depletion region occupy all the lowly doped drain region. Once this condition is reached, the increase in the breakdown voltages is slower.

The high-voltage p-type MOSFETs experience decreases in their breakdown voltages at the highest neutron fluences used in this experiment. This can be attributed to the positive charge in the oxide. When the charge in the oxide increases, punchthrough may occur at lower voltages, and the breakdown voltage may eventually decrease.

Another limiting factor is the termination structure. Most devices have a highly doped ring surrounding the device called a channel stop. The purpose of this ring is to keep the depletion region from the edge of the chip. The ring is an n-type diffusion for an n-channel MOSFET (see figure 5.3) and p-type for a p-channel MOSFET [31]. For most of the commercial devices, it is likely that the channel stop is placed far enough from the termination structure to just accommodate the voltage rating of the devices. Thus, when the breakdown voltage is increased due to the decrease of the mean free path, the depletion region will eventually reach it. This will also limit the increase in the breakdown voltage.

In the p-channel MOSFETs, with positive oxide charge causing the depletion region to extend outward, the channel stop is reached sooner than with no positive oxide charge. The channel stop will deflect the curvature of the equipotential lines close to it. This may further limit the breakdown voltage increase.

In the n-type MOSFETs, with the oxide charge bending the depletion region inward, the equipotential lines will touch the channel stop at a higher voltage compared to the p-type MOSFETs. Also, the n-type devices experience a slower increase in their

breakdown voltages due to the differences in the change in the mean free path. These factors explain why the pMOSFET ΔBV stops increasing at 10^{14} cm^{-3}, while they only slow down the increase in the nMOSFET (see figure 5.1).

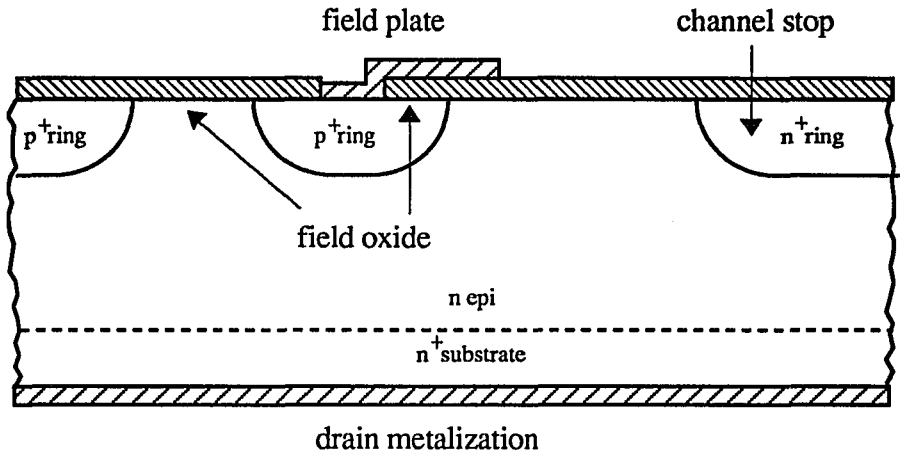

Figure 5.3 Channel stop at the end of a termination structure

5.5 Mathematical Model

Empirical models of the neutron irradiation effect on the breakdown voltage based on the experimental and simulation results have been developed; namely models for the breakdown voltage and ionization coefficients. These models are useful in predicting the breakdown voltage of a power MOSFET after a certain neutron fluence.

5.5.1 Breakdown Voltage Model

A relation between the breakdown voltage BV of a power MOSFET and the cumulative neutron fluence Φ was developed. The model was derived using the experimental results of chapter 3.

Figures 5.3 and 5.4 show the relation between the normalized breakdown voltage change ΔBV and the neutron fluence. They show some effects of the localized oxide charge as discussed in section 5.2. At low fluence levels, the effect of the oxide charge is significant. At higher fluence levels, where the effect of the dislocations is larger than the effect of the oxide charge, the relation is almost linear for each device. The general relation can be written empirically as

$$\frac{\Delta BV(\Phi)}{BV_{init}} = \nu\Phi + C_\gamma \qquad (5.1)$$

where ν is the linear slope and C_γ is the constant correctional factor due to the oxide charge and other non-idealities. Curve fits are performed for each device, and table 5.1 lists all ν and C_γ values for the devices in this experiment. These constants are found after omitting some data that have been significantly affected by the aforementioned limiting factors, namely the high-voltage-MOSFET data points at high fluences.

From figures 5.4 and 5.5, and especially from table 5.1, it is observed that the effect of neutron irradiation is a function of initial breakdown voltages. Thus, in figures 5.6 and 5.7, the slopes ν are plotted versus the initial breakdown voltage of the devices. Figure 5.6 shows an approximately linear relation for all points except one. This one point belongs to one of the two highest-rated n-type MOSFETs in the experiment. High-voltage devices

are very sensitive to oxide charge, and also may be affected by the device dimensions and the termination-structure limiting factors.

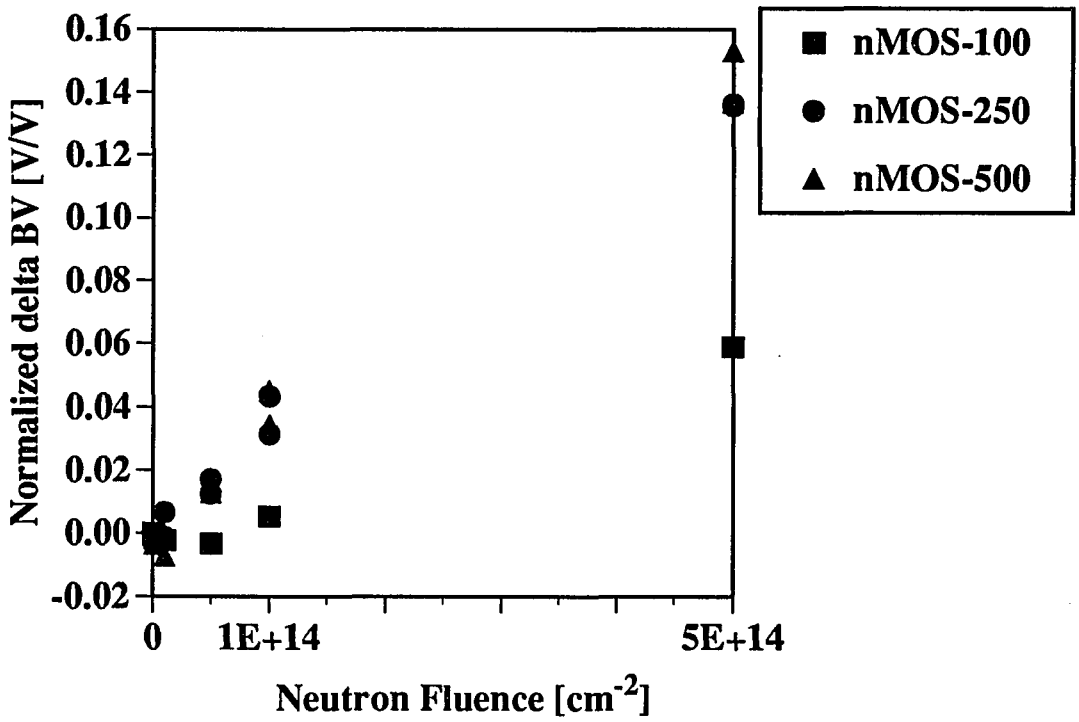

Figure 5.4 Normalized change in breakdown voltage versus neutron fluence for nMOSFET devices

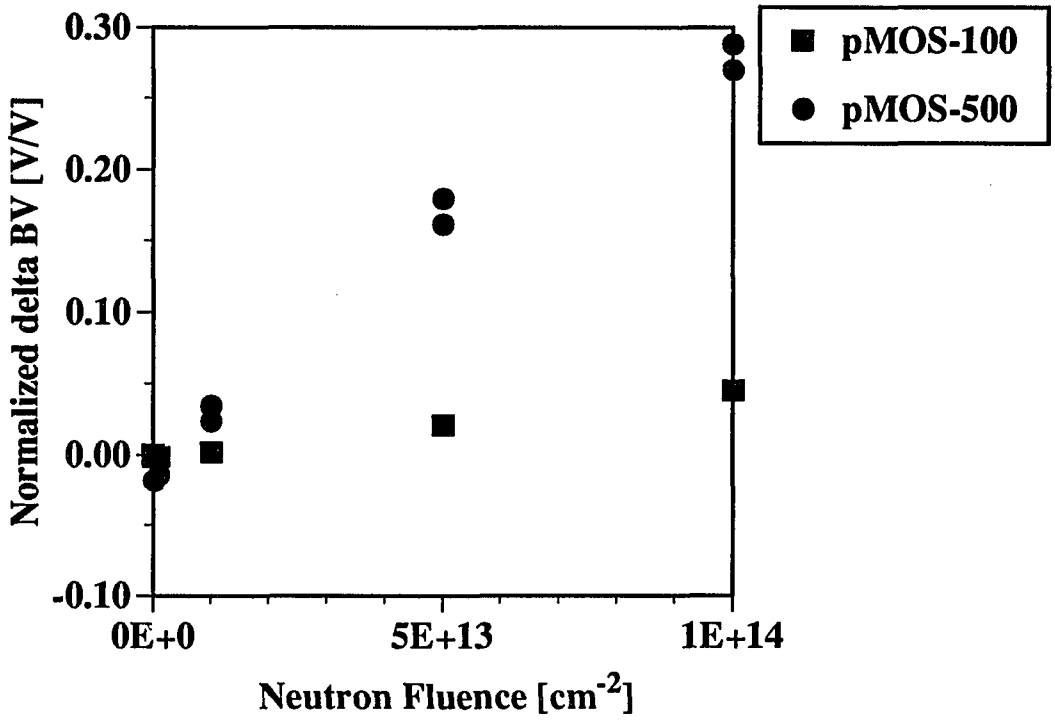

Figure 5.5 Normalized change in breakdown voltage against neutron fluence for pMOSFET devices

Model Number	BV_{init}	ν(fV.cm^2/V)	C_γ(mV/V)
MTM12N10	117.0 V	0.125	-4.294
MTM10N25-1	314.5 V	0.283	1.936
MTM10N25-2	310.7 V	0.302	0.626
2N6759	427 V	0.434	-3.219
IRF440-1	561 V	0.517	-3.975
IRF440-2	551 V	0.407	-6.748
MTM8P10	114.3 V	0.653	-7.549
MTM2P45	569 V	4.635	0.629
MTM2P50-1	551 V	3.653	-13.294
MTM2P50-2	552 V	3.873	-9.368

Table 5.1 ν and C_γ of the devices of the neutron irradiation experiment

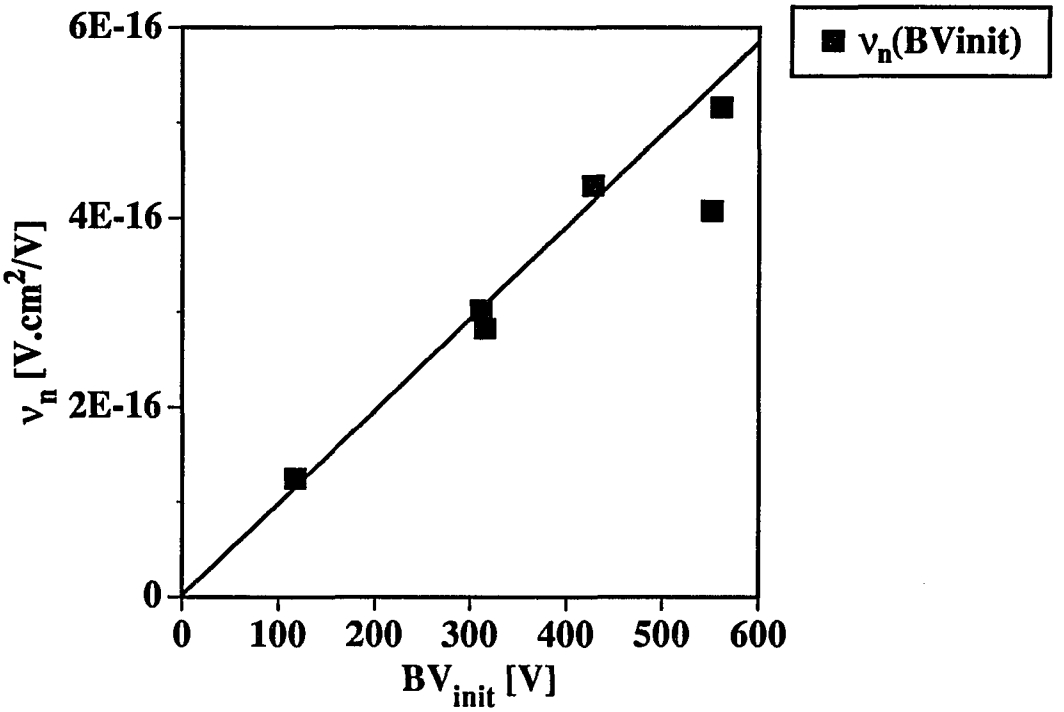

Figure 5.6 ν versus initial breakdown voltage of nMOSFETs

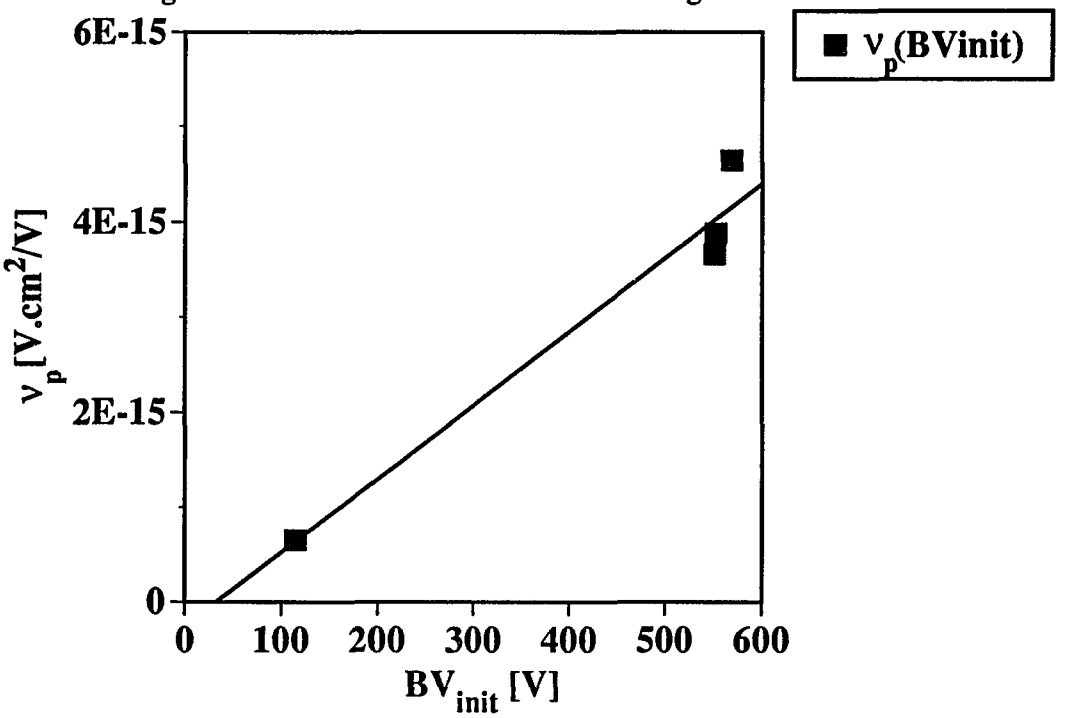

Figure 5.7 ν versus initial breakdown voltage of pMOSFETs

There are four p-type devices that make up points in figure 5.7. The points are not well spread, but since the n-type devices in figure 5.6 show a linear relationship, it is reasonable to assume that the linear relation also applies for ν versus breakdown voltages of p-type MOSFETs.

The linear curve fits in figures 5.6 and 5.7 are

$$\nu_n = \nu_{n1} BV_{init} + \nu_{n0} \qquad (5.2\text{-a})$$

$$\nu_p = \nu_{p1} BV_{init} + \nu_{p0} \qquad (5.2\text{-b})$$

where the subscripts n and p refer to the type of the lowly-doped epi-layer material and the channel, and

$$\nu_{n1} = 9.73 \times 10^{-19} \text{ cm}^2/\text{V}$$

$$\nu_{n0} = 1.51 \times 10^{-18} \text{ cm}^2$$

$$\nu_{p1} = 7.74 \times 10^{-18} \text{ cm}^2/\text{V}$$

$$\nu_{p0} = -2.51 \times 10^{-16} \text{ cm}^2 .$$

ν_{n0} and ν_{p0} are the zero-volt intercepts. For the range of high voltage devices in these experiments, the ν_{n0} and ν_{p0} terms can be neglected. Thus, equations (5.2), combined with equation (5.1), give

$$\frac{\Delta BV(\Phi)}{BV_{init}} = \nu_1 BV_{init} \Phi + C_\nu \; . \qquad (5.3)$$

If only neutron fluence without any concomitant gamma radiation is considered, and the devices follow ideal parallel-plane structure behavior (C_γ=0), the equation (5.3) can be written as

$$\frac{\Delta BV(\Phi)}{BV_{init}} = v_1 BV_{init}\Phi \tag{5.4}$$

or

$$BV(\Phi) = v_1 (BV_{init})^2 \Phi + BV_{init} \, . \tag{5.5}$$

Equation (5.5) can be easily used to predict the breakdown voltage of a power MOSFET after a given neutron fluence, given the initial breakdown voltage. This empirical model does not apply if the lower doped drain region is already completely depleted. Equation (5.5) is compared to the experimental data in figures 5.8 and 5.9. They demonstrate excellent agreement, except for the high-fluence neutron-irradiated p-type MOSFETs rated at 450 V and 500 V. These devices had been affected by the device limiting structure.

For comparison purposes, figures 5.10 and 5.11 show the predictions of the carrier removal model of equation (2.5) and the experimental data. The carrier removal model shows very inaccurate predictions because the model has assumed that traps in the bulk region and in the depletion region have the same rate in removing carriers.

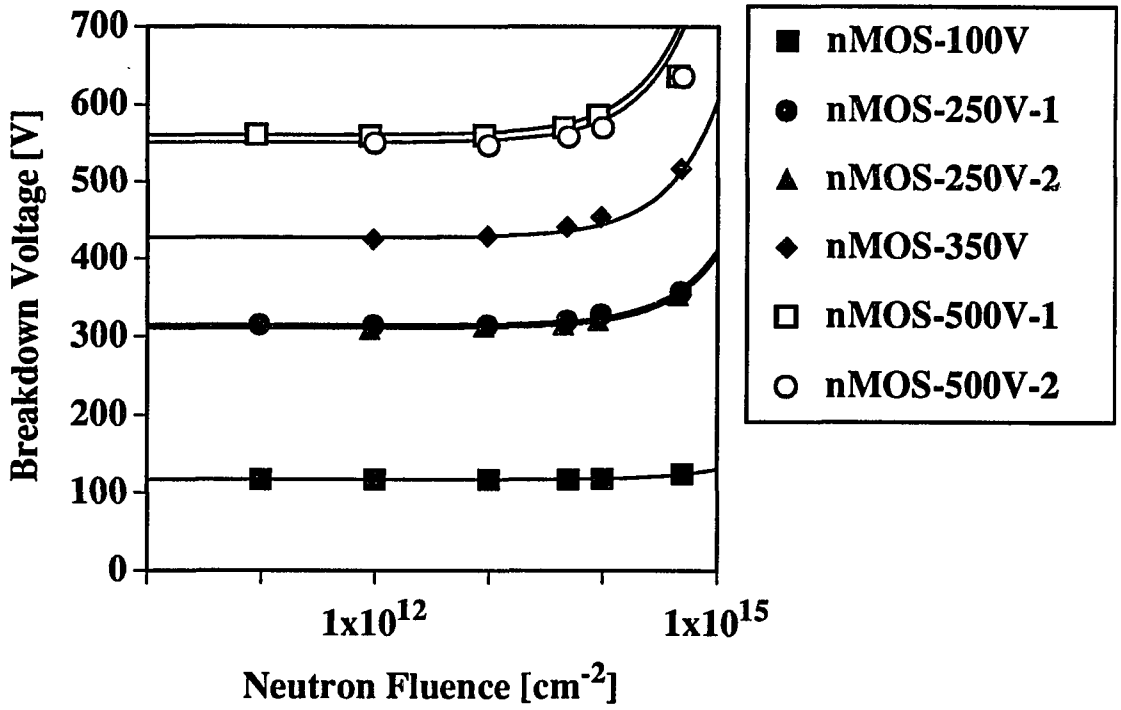

Figure 5.8 Breakdown voltage model: n-type MOSFETs

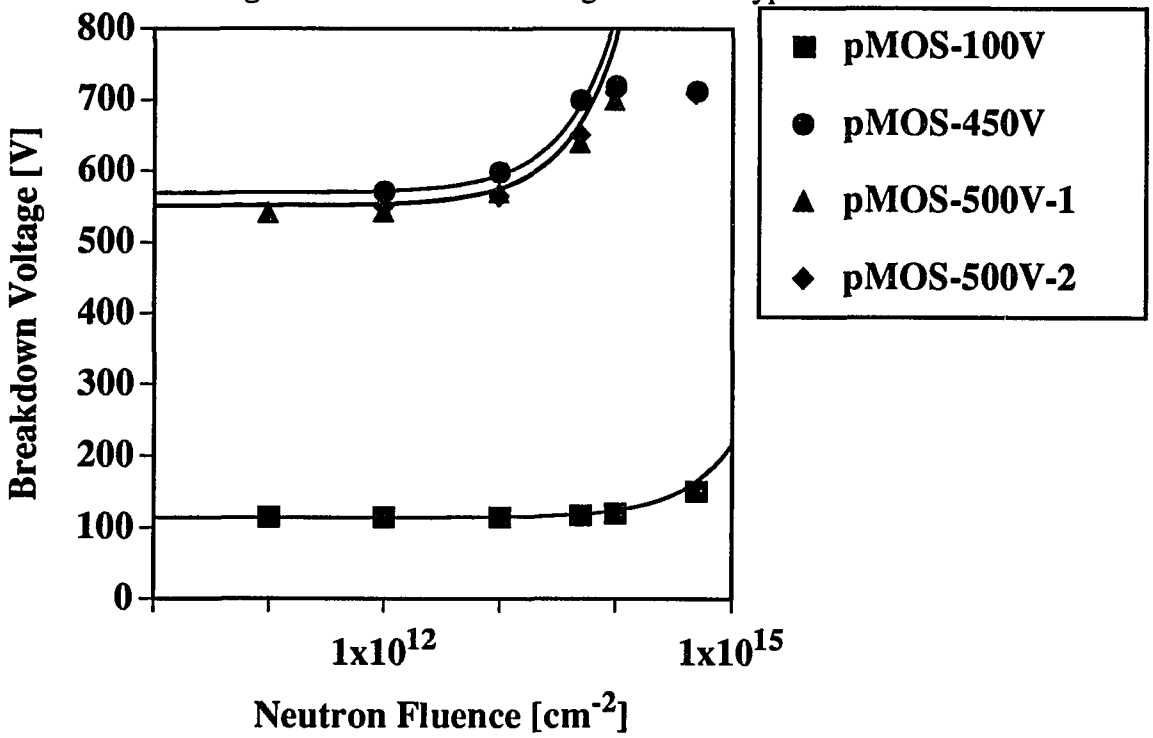

Figure 5.9 Breakdown voltage model: p-type MOSFETs

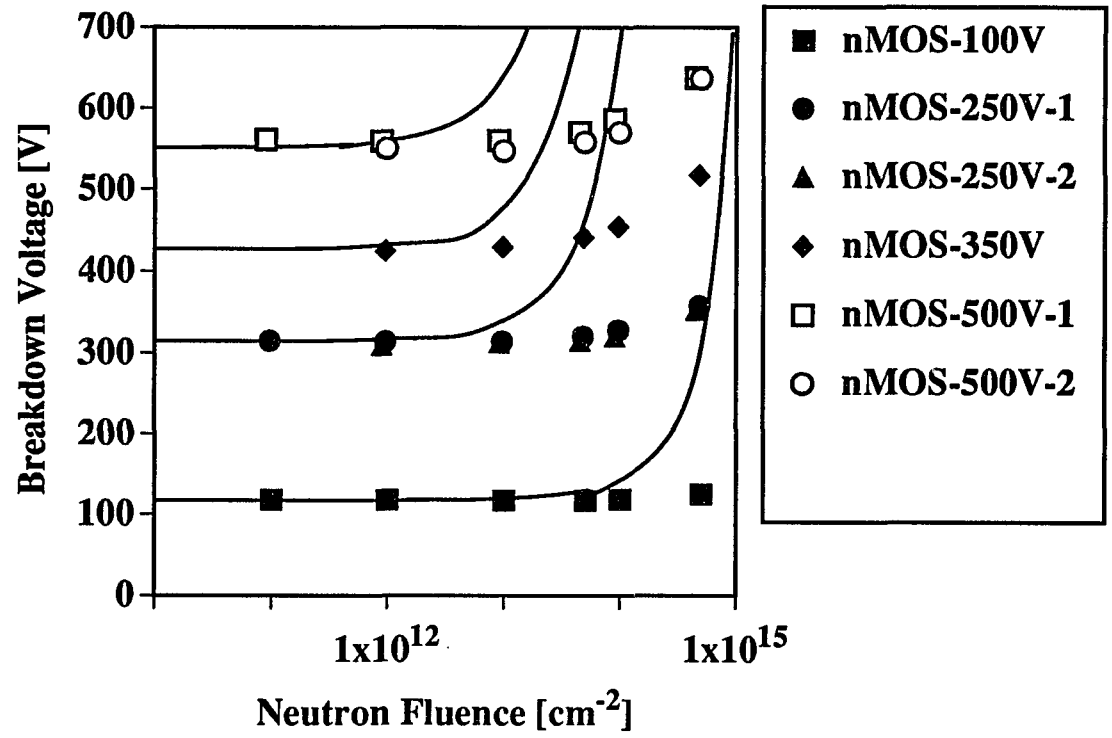

Figure 5.10 Carrier removal model: n-type MOSFETs

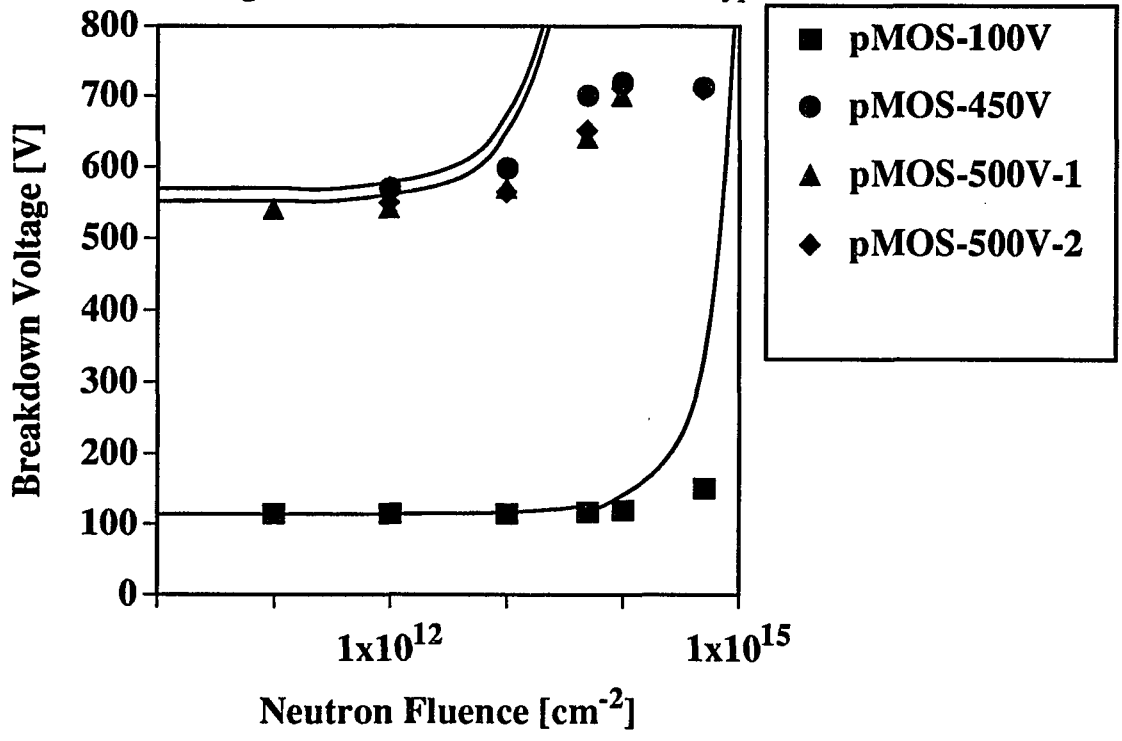

Figure 5.11 Carrier removal model: p-type MOSFETs

5.5.2 Ionization Coefficient Model

The breakdown voltage model of equation (5.5) is only a first degree model. It does not include positive charge effects on the equipotential lines near the oxide-silicon interface. It does not take the device structure into account either. In this section, a model will be developed to make it possible to incorporate neutron irradiation effect into a device simulation: ionization coefficient model. Along with the model, the positive oxide charge and device structure effects can be simulated using S-PISCES 2B or other device simulations.

In chapter 4, S-PISCES 2B simulations give a linear relation between the parallel-plane $\frac{\Delta BV}{BV}$ and $\frac{\Delta b}{b}$. The linear relation of equation (4.2) can be modified to

$$b(\Phi) = \left(1 + \frac{\Delta BV(\Phi)}{S \times BV_{pp}}\right) b(0) \ . \qquad (5.6)$$

This equation relates a Van Overstraeten and De Man constant b(0), a slope constant S, a parallel-plane breakdown voltage BV_{pp}, and the change of BV due to a neutron fluence Φ to the b coefficient as a function of Φ. Some of these variables in the right hand side of equation (5.6) are not readily available as inputs. S is a constant that is found to be 1.724, and b(0) is a constant available in S-PISCES 2B device simulation. Φ is the total neutron fluence. However, a breakdown voltage is usually an output of a device simulation. Its value is not known at the beginning of the simulation. Equation (5.6) must be modified.

Devices in this experiment use a multiple-ring structure. The use of multiple rings is to achieve breakdown voltage very close to its parallel-plane breakdown voltage value.

Assuming that $BV_{init} = BV_{pp}$, where $BV_{pp}=5.34x10^{13}N_{dop}^{-3/4}$, equation (5.6) can be combined with equation (5.4) to give

$$b(\Phi)=\left[\frac{\nu_2 N_{dop}^{-3/4}\Phi}{S}+1\right]b(0) \qquad (5.7)$$

where

$$\nu_{n2} = 5.20 \times 10^{-5}\ cm^{-1/4}$$

for n-type material, and

$$\nu_{p2} = 4.13 \times 10^{-4}\ cm^{-1/4}$$

for p-type material.

Equation (5.7) contains only readily available inputs to a device simulation. This model is an empirical model that describes the atomic dislocations due to neutron radiation, and it is the first ionization coefficient model that considers the change in mean free path due to the neutron radiation.

CHAPTER 6

SUMMARY AND CONCLUSIONS

The effect of neutron irradiation on power MOSFETs can be divided into three regions. This is especially true for the high-voltage p-type MOSFETs in this experiment. Figure 6.1 shows the three regions. The boundaries of these three regions are device dependent.

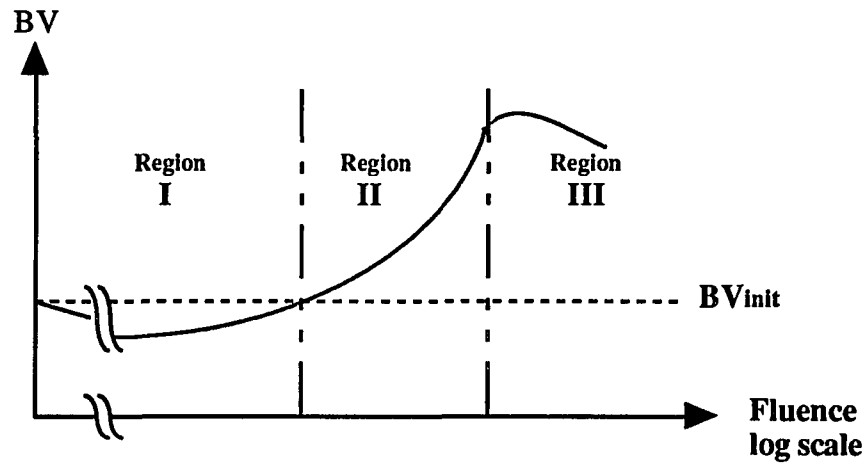

Figure 6.1 Neutron irradiation effect on the power MOSFET

In the first region, the localized positive oxide charge and the decrease in the mean free path contribute. The positive oxide charge disturbs the equipotential lines in the depletion region close to the Si-SiO_2 interface. The change in the equipotential lines decreases the breakdown voltages of the n-channel MOSFETs. In the p-channel

MOSFETs, small amounts of positive oxide charge increase the breakdown voltage, while large amounts may or may not enhance the breakdown voltages, and may actually cause the breakdown voltages to decrease [17]. The decrease in mean free path reduces the possibility of carriers gaining enough energy to start impact ionization, reduces the ionization rate, and increases the breakdown voltage. Depending on the type of the MOSFET and which effect is stronger, the breakdown voltage of the device can increase or decrease slightly.

In the second region, the decrease of the mean free path dominates. All transistors show an upward trend in their breakdown voltages. The number of dislocations is relatively high. The effect of the change in mean free path on the breakdown voltage is bigger than changes caused by the positive oxide charge. Assuming no change in ionization energy, as little as 4% change in the mean free path gives the necessary breakdown voltage change experienced by a 100-volt nMOSFET after neutron irradiation of $5x10^{14}$ cm^{-2}. There is a factor between 2 and 5 difference in the rate of change of the mean free path of the n-type and p-type silicon.

Region III is only seen for relatively high-voltage-rating pMOSFETs. In this region, the breakdown voltage decreases. This is believed to be due to the limitation of the epi-layer thickness or the termination structure.

Two empirical models have been developed. One model relates the change in the breakdown voltage and the fluence. This relation can be used to approximate the effect of neutron irradiation on power-MOSFET breakdown voltages:

$$BV(\Phi) = v_1 (BV_{init})^2 \Phi + BV_{init} \tag{6.1}$$

where v_1 is a neutron irradiation constant for n- or p-type devices, and BV_{init} is the initial breakdown voltage before the radiation. The values of the constants are listed in table 6.1.

Type	$v_2(cm^{-1/4})$	$v_1(cm^2/V)$
n-type	5.20×10^{-5}	9.73×10^{-19}
p-type	4.13×10^{-4}	7.74×10^{-18}

Table 6.1 Neutron irradiation constants

The other model considers the effect of neutron irradiation on the ionization rate:

$$b(\Phi) = \left[\frac{v_2 N_{dop}^{-3/4} \Phi}{S} + 1 \right] b(0) \tag{6.2}$$

where

$$S = \left(\frac{\Delta BV}{BV_{pp}} \right) \Big/ \left(\frac{\Delta b}{b(0)} \right) = 1.724 \tag{6.3}$$

and v_2 for n- and p-type devices are listed in table 6.1.

The change in mean free path due to the atomic dislocations in the depletion region explains the increase of the breakdown voltage after prolonged neutron irradiation. The

relation between the change in breakdown voltage ΔBV and the neutron fluence Φ is shown by equation (6.1). This relation can be utilized to estimate the change in the breakdown voltages for power MOSFET devices under neutron irradiation. The relation suggests an increase in the breakdown voltage after prolonged irradiation. This advantage trades off with the increase of the bulk silicon resistivity due to carrier removal according to equation (2.1). The increase in resistivity causes the on-resistance to increase.

A relation for the ionization rate as a function of the neutron irradiation is also proposed. This relation is derived from a limited amount of data. Future work is required to refine this relationship. The relation is shown in equation (6.2). This equation could be implemented in PISCES for a neutron irradiation model with minor work. Chynoweth's law is already used in the model. The Van Overstraeten and De Man coefficients are the default values in Selberherr's model of S-PISCES 2B. A modification can be introduced in the model that involves adding 2 constants (ν_2, and ν_1) for each type of material plus a slope constant S. The correction factor in equation (5.3) is not needed in PISCES because oxide charge could be introduced in the material using the available model and device structures are part of the simulation. Along with equation (6.2), the carrier removal model of equations (2.3) can also be introduced to account for the change in the resistivity of the bulk material. The two models need only one single variable input: total neutron fluence Φ.

REFERENCES

[1] P. L. Hower, "A Comparison of Bipolar and Field Effect Transistor as Power Switches," Power Conversion International, vol. 7, no. 1, p 45, 1981.

[2] D.A. Grant and J. Gowar, *POWER MOSFETs: Theory and Applications*, John Wiley & Sons, New York, 1989.

[3] R. A. Meyers, *Encyclopedia of Physical Science and Technology*, Academic Press Inc., Orlando, Florida, 1987.

[4] B. J. Baliga, *Modern Power Devices*, John Wiley & Sons, New York, 1987.

[5] S. M. Sze, *Physics of Semiconductor Devices*, John Wiley & Sons, New York, 1981.

[6] A. G. Chynoweth, Uniform Silicon p-n Junctions. II. Ionization Rates for Electrons, *J. Appl. Phys.*, vol. 31, no. 7, pp. 1161-1165 , 1960.

[7] J.L. Moll and R. Van Overstraeten, Charge Multiplication in Silicon p-n Junctions, *Solid State Electron.*, vol. 6, no. 2, pp. 147-157, 1963.

[8] C.A. Lee, R.A. Logan, R.L. Latdorf, J.J. Kleimack and W.W. Wiegmann, Ionization Rates of Holes and Electrons in Silicon, *Phys. Rev.*, vol. 134, no. 3A, pp. A761-A773, 1964.

[9] R. Van Overstraeten and H. De Man, Measurement of the Ionization Rates in Diffused silicon p-n junctions, *Solid State Electron*, vol. 13, no. 5, pp. 583-608, 1970.

[10] V. A. K. Temple and M. S. Adler, Calculation of the Diffusion Curvature Related Avalanche Breakdown in High Voltage Planar p-n Junctions, *IEEE Trans. Electron Devices*, vol. ED-22, no. 10, pp. 910-916 , 1975.

[11] W. Shockley, Problems Related to p-n Junctions in Silicon, *Solid State Electron.*, vol. 2, no. 1, pp. 35-67, 1961.

[12] M.S. Adler, V.A.K. Temple, A.P. Ferro, and R.C.Rustay,Theory and Breakdown Voltage for Planar Devices with a Single Field Limiting Ring, *IEEE Trans. Electron Devices*, vol. ED-24, no. 2, pp. 107-113, 1977.

[13] K.P. Brieger, W. Gerlach, and J. Pelka, Blocking Capability of Planar Devices with Field Limiting Rings, *Solid State Electron.*,vol. 26, no.8, pp. 739-745, 1983.

[14] W. Tantaporn and V.A.K. Temple, Multiple-Zone Single-Mask Junction Termination Extension - A High-Yield Near-Ideal Breakdown Voltage

Technology, *IEEE Trans. Electron Devices*, vol. ED-34, no. 10, pp 2200-2210, 1987.

[15] S. Ahmad and J. Akhtar, A Proposed Planar Junction Structure with Near-Ideal Breakdown Characteristics, *IEEE Trans. Electron Devices Letters*, vol. EDL-6, no. 9, pp. 465-467, 1985.

[16] S.L. Kosier, R.D. Schrimpf, K.F. Galloway, and F.E. Cellier, Predicting Worst-Case Charge Buildup in Power-Device Field Oxides, *IEEE Trans. Nucl. Sci.*, vol. 38, no. 6, pp. 1383-1390, 1991.

[17] S.L. Kosier, R.D. Schrimpf, F.E. Cellier, and K.F. Galloway, The Effects of Ionizing Radiation on the Breakdown Voltage of p-Channel Power MOSFETs, *IEEE Trans. Nucl. Sci.*, vol. 37, no.6, pp. 2076-2082, 1990.

[18] J.R. Srour, "Radiation effects," in *Radiation Effects on and Dose Enhancement of Electronic Materials*, J.R. Srour, D.M. Long, D.G. Millward, R.L. Fitzwilson, and W.L. Chadsey, Noyes Publications, New Jersey, 1984.

[19] F. B. McLean, "Interactions of Hazardous Environments with Electronic Devices," in *Hardening Semiconductor Components Against Radiation and Temperature*, W.R. Dawes, Jr., F.B. McLean, P.A. Robinson, Jr., and J.J. Silver, Noyes Data Corporation, New Jersey, 1989.

[20] G.C. Messenger and M.S. Ash, *The Effects of Radiation on Electronic Systems*, Van Nostrand Reinhold Company, New York, 1986.

[21] D.S. Billington, J.H. Crawford,Jr., *Radiation Damage in Solids*, Princeton UniversityPress, New Jersey, 1961.

[22] J.W. Corbett, "Electron Radiation Damage in Semiconductors and Metals," in *Solid State Phys.*, vol. suppl. 7, F. Seitz and D. Turnbull (eds.), Academic Press, New York, 1966.

[23] M.G. Buehler, "Design Curves for Predicting Fast-Neutron-Induced Resistivity Changes in Silicon," *Proc. IEEE (Letters)*, vol. 56, no. 10, pp. 1741-1743, October 1968.

[24] H.J. Stein, *Introduction Rate of Electrically Active Deffects in Silicon by Nuclear Radiation*, Sandia Corp., Albuquerque, N. Mex., SC-R-65-938, July1965, cited in "Design Curves for Predicting Fast-Neutron-Induced Resistivity Changes in Silicon," M.G. Buehler, *Proc. IEEE (Letters)*, vol. 56, no. 10, pp. 1741-1743, October 1968.

[25] O.L. Curtis, Jr., R.F. Bass, and C.A. Germano, *Impurity Effects in Neutron Irradiated Silicon and Germanium*, Harry Diamond Labs., Washington, D.C., Rept. 235-1, November 1965, cited in "Design Curves for Predicting Fast-

Neutron-Induced Resistivity Changes in Silicon," M.G. Buehler, *Proc. IEEE (Letters)*, vol. 56, no. 10, pp. 1741-1743, October 1968.

[26] G.W. Neudeck, "The PN Junction Diode," in *Modular Series on Solid State Devices*, vol. II, G.W. Neudeck and R.F. Pierret (eds.), Addison-Wesley Publishing Company, New York, 1989.

[27] L. Reggiani, "General Theory," in *Hot-Electron Transport in Semiconductor*, L. Reggiani (ed.), *Topics in Applied Physics*, vol.58, Springer-Verlag, Berlin, 1985.

[28] F. B. McLean, H.E. Boesch, Jr., and T.R. Oldham, "Electron-Hole Generation, Transport, and Trapping in SiO_2," in *Ionizing Radiation Effects in MOS Devices and Circuits*, T.P. Ma and P.V. Dressendorfer (eds.), A Wiley-Interscience Publication, New York, 1989.

[29] Silvaco International, S-PISCES 2B User's Manual, ver. 5.1, 1992.

[30] S. Selberherr, *Analysis and Simulation of Semiconductor Devices*, Springer-Verlag, New York, 1984.

[31] V.A.K. Temple and W. Tantraporn, "Junction Termination Extension for Near-Ideal Breakdown Voltage in p-n Junctions," *IEEE Trans. Electron Devices*, vol. ED-33, no. 10, pp. 1601-1608, 1977.